Schweizerische Eidgenossenschaft
Confédération suisse
Confederazione Svizzera
Confederaziun svizra

Federal Department of the Environment,
Transport, Energy and Communications DETEC

Swiss Federal Office of Energy
Energy Research and Cleantech

Interim report from 31 October 2024

BEACH

Bedretto Energy Storage and Circulation of Geothermal Energy

Source: SRF news 10vor10, 02.08.2024, coloured water flowing in a fracture in Bedretto Laboratory

Publisher:
Swiss Federal Office of Energy SFOE
Energy Research and Cleantech
CH-3003 Berne
www.energy-research.ch

Subsidy recipients:
SUPSI
University of Applied Sciences and Arts
of Southern Switzerland
Via Flora Ruchat-Roncati 15
6850 Mendrisio

GeoEnergie Suisse
Reitergasse 11
8004 Zürich

AET - Azienda Elettrica Ticinese
El Stradún 74
6513 Monte Carasso

Authors:
Maren Brehme, Marian Hertrich, Tsubasa Onishi, Mahmoud Hefny, ETH Zurich, mbrehme@ethz.ch
Andres Alcolea, GES, a.alcolea@geo-energie.ch
Filippo Schenker, Alessia Grignaschi, Simone.Zavattoni@supsi.ch, SUPSI, Filippo.Schenker@supsi.ch

SFOE project coordinators:
Prof. Martin O. Saar, Prof. Hansruedi Maurer, saarm@ethz.ch
Jean-Pierre Candeloro, SUPSI
Peter Meier, p.meier@geo-energie.ch
Edy Losa, edy.losa@aet.ch

SFOE contract number: SI/502817-01

The authors bear the entire responsibility for the content of this report and for the conclusions drawn therefrom.

Summary

In the BEACH project, we propose tackling the challenges of the Swiss energy transition with demonstrating a new technology for storing and retrieving energy in the subsurface: Fractured Thermal Energy Storage (FTES). This could be a key component for providing baseload energy to compensate for seasonal phases of energy demand and surplus. To our knowledge, this is the first attempt of energy storage in crystalline rock, which is particularly interesting for Switzerland, because large parts of the Swiss subsurface include this rock type. We will test several scenarios on their suitability for energy storage, and we will demonstrate that this can be achieved in an efficient and safe manner with appropriate monitoring techniques.

Here, we report on the first phase of the project. Using numerical modelling approaches, we show the feasibility and efficiency of FTES with a single hole scenario at the Bedretto Lab test site. We demonstrate that with realistic injection rates of 200 l/min of 60°C water, the efficiency can be > 70%. Based on these numerical results, we present an experimental setup that will be implemented in the next phase of the project at our test site in the Bedretto Lab. First trials are expected to start in early 2025.

Furthermore, we provide three conceptual case studies, with which we show that our concept is applicable to a range of potential sites in Switzerland. With a comprehensive fracture analysis at the Vallemaggia site, we demonstrate the potential usefulness of this location for FTES purposes. Furthermore, show that the results obtained at the Bedretto Lab can be transferred to a site near Schaffhausen. Finally, we make use of a newly established industry collaboration in Northern Switzerland to prove the economic viability of FTES.

Zusammenfassung

Im Projekt BEACH schlagen wir vor, die Herausforderungen der Schweizer Energiewende anzugehen, indem wir eine neue Technologie zur Speicherung und Entnahme von Energie im Untergrund demonstrieren: Fractured Thermal Energy Storage (FTES). Dies könnte eine Schlüsselkomponente für die Bereitstellung von Grundlastenergie sein, um saisonale Phasen von Energiebedarf und -überschuss auszugleichen. Unseres Wissens ist dies der erste Versuch der Energiespeicherung in kristallinem Gestein, was für die Schweiz besonders interessant ist, da große Teile des Schweizer Untergrunds aus diesem Gesteinstyp bestehen. Wir werden mehrere Szenarien auf ihre Eignung zur Energiespeicherung testen und zeigen, dass dies mit geeigneten Überwachungstechniken effizient und sicher erreicht werden kann.

Hier berichten wir über die erste Phase des Projekts. Mithilfe numerischer Modellierungsansätze zeigen wir die Machbarkeit und Effizienz von FTES mit einem Einzellochszenario auf dem Testgelände des Bedretto-Labors. Wir zeigen, dass bei realistischen Injektionsraten von 200 l/min 60 °C heißem Wasser die Effizienz über 70 % liegen kann. Basierend auf diesen numerischen Ergebnissen präsentieren wir einen Versuchsaufbau, der in der nächsten Phase des Projekts an unserem Teststandort im Bedretto-Labor umgesetzt wird. Erste Versuche werden voraussichtlich Anfang 2025 beginnen.

Darüber hinaus stellen wir drei konzeptionelle Fallstudien vor, mit denen wir zeigen, dass unser Konzept auf eine Reihe potenzieller Standorte in der Schweiz anwendbar ist. Mit einer umfassenden Bruchanalyse am Standort Vallemaggia demonstrieren wir die potenzielle Nützlichkeit dieses Standorts für FTES-Zwecke. Darüber hinaus zeigen wir, dass die im Bedretto-Labor erzielten Ergebnisse auf einen Standort in der Nähe von Schaffhausen übertragen werden können. Schließlich nutzen wir eine neu gegründete Industriekooperation in der Nordschweiz, um die wirtschaftliche Rentabilität von FTES nachzuweisen.

Résumé

Dans le cadre du projet BEACH, nous proposons de relever les défis de la transition énergétique suisse en démontrant une nouvelle technologie de stockage et de récupération d'énergie dans le sous-sol : le stockage d'énergie thermique fracturé (FTES). Il pourrait s'agir d'un élément clé pour fournir de l'énergie de base afin de compenser les phases saisonnières de demande et de surplus d'énergie. À notre connaissance, il s'agit de la première tentative de stockage d'énergie dans la roche cristalline, ce qui est particulièrement intéressant pour la Suisse, car de grandes parties du sous-sol suisse comprennent ce type de roche. Nous testerons plusieurs scénarios sur leur adéquation au stockage d'énergie, et nous démontrerons que cela peut être réalisé de manière efficace et sûre avec des techniques de surveillance appropriées.

Nous rendons compte ici de la première phase du projet. En utilisant des approches de modélisation numérique, nous démontrons la faisabilité et l'efficacité du FTES avec un scénario de trou unique sur le site d'essai du Bedretto Lab. Nous démontrons qu'avec des débits d'injection réalistes de 200 l/min d'eau à 60°C, l'efficacité peut être > 70 %. Sur la base de ces résultats numériques, nous présentons un dispositif expérimental qui sera mis en œuvre dans la prochaine phase du projet sur notre site d'essai au laboratoire Bedretto. Les premiers essais devraient commencer début 2025.

En outre, nous fournissons trois études de cas conceptuelles, avec lesquelles nous montrons que notre concept est applicable à une série de sites potentiels en Suisse. Avec une analyse complète des fractures sur le site de Vallemaggia, nous démontrons l'utilité potentielle de cet emplacement pour les FTES. En outre, nous démontrons que les résultats obtenus au laboratoire Bedretto peuvent être transférés sur un site près de Schaffhouse. Enfin, nous utilisons une collaboration industrielle nouvellement établie dans le nord de la Suisse pour prouver la viabilité économique du FTES.

Contents

List of tables

List of abbreviations

SFOE	Swiss Federal Office of Energy
BEACH	Bedretto Energy Storage and Circulation of Geothermal Energy

1 Introduction

1.1 Context and motivation

The main objective of the BEACH project is to demonstrate the feasibility and technical requirements for energy storage in fractured crystalline rocks: Fractured Thermal Energy Storage (FTES). This is a new technology with great potential to support the energy transition in Switzerland (Figure 1). To keep the Swiss net-zero emission target of the Federal Council (2021) by 2050, new technologies need to enter the energy market in addition to renewable sources already available. In this context, energy storage is an increasingly important topic in times of energy excess during certain periods and energy shortage during other periods (Energy Perspectives 2050+). Recent developments in the energy market call for a solar electricity production cut because of lack of capacity in the grid (SRF, 8.11.2024). To avoid such inefficient approaches, excess energy could be stored underground.

Subsurface storage of energy in suitable geological units at shallow, intermediate and greater depths can play an important role. Geothermal reservoirs, adequate for energy storage, are present in different geological environments and at various depths and temperatures. In Switzerland, potential geothermal reservoirs are located in sedimentary rocks in the Molasse basin and in fractured crystalline rocks. The Forsthaus project is the first example in Switzerland, where heat will be stored at 500m in deep sandstones (Link et al., 2020). However, a large part of the Swiss underground is made of fractured crystalline rocks. Conceptual studies on FTES investigated different aspects of thermal energy storage. Operational parameters are key to avoiding early thermal breakthrough, optimally using the fracture geometry and matrix interaction, and adapting to the rock properties (De La Bernardie et al. (2018); Klepikova et al. (2021); Zhou et al. (2022); Knobloch et al. (2022)).

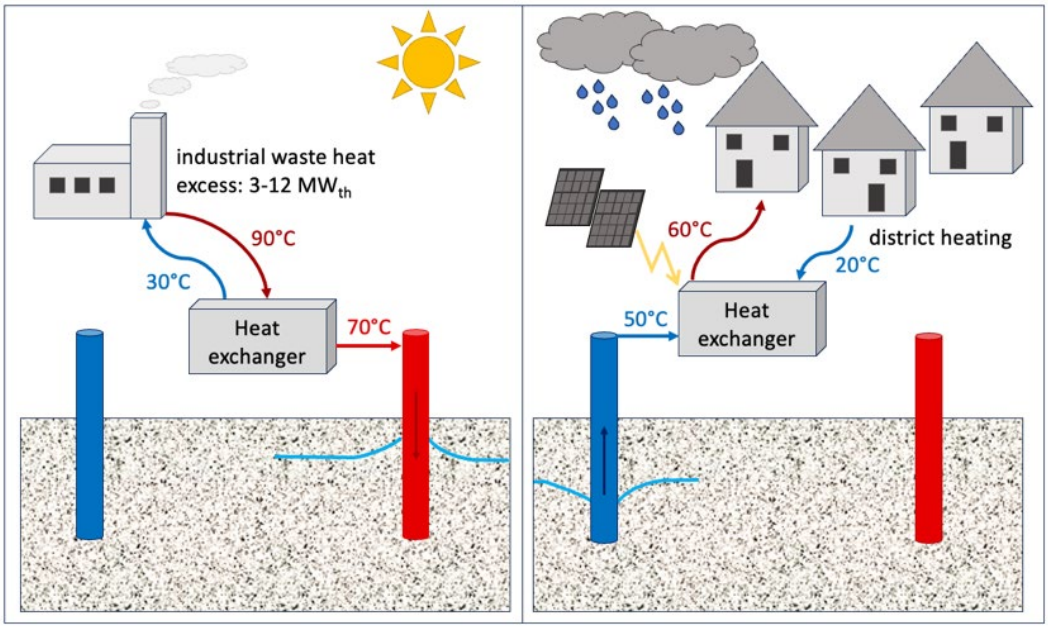

Figure 1 Concept of energy subsurface storage in summer by injecting excess heat via a wellbore into the underground (left) and extraction of the heat during winter to feed district heating grids (right)

Although the results of these conceptual studies are encouraging, we see an urgent need (i) to further analyze the theoretical feasibility of energy storage in fractured crystalline rocks, (ii) to investigate the economic possibilities and limitations of such an endeavor, and, most importantly, (iii) to demonstrate

its practical feasibility by means of a realistic demonstrator project. In brief, the overall outcome of the project is an answer to ‘How can heat storage in fractured crystalline rocks support the energy transition in Switzerland towards the net-zero goal?’.

1.2 Project objectives

In the BEACH pilot and demonstration project the possibilities to store heat in fractured crystalline rocks will be investigated in three incremental phases with measurable targets. In Phase I, numerical and conceptual studies on the feasibility and economy of FTES will be conducted, including a conceptual design of the first experiments. The first experiments, in a single-hole setup, will be conducted in Phase II. Various setups, storage cycles, flow rates and temperatures will be tested during the experiments in the BedrettoLab. In Phase III, two-hole experiments will be conducted to test the circulation of the injected warm water in the subsurface.

The project is organized in four work packages, which build upon each other and interact by sharing data, information and predictive scenarios for the real-scale tests (Figure 1). In the first work package (WP1) the general feasibility of the concept is numerically tested, and reservoir models are used for process understanding pre-, syn- and post-operations. The second work package (WP2) includes the test design phase, where the outcomes of WP1 are used for detailed planning of the tests and setting up the infrastructure. The third work package (WP3) entails the conduction of the real-scale test activities in the BedrettoLab including preparational work, onsite engineering and monitoring activities. Finally, the fourth work package (WP4) is responsible for scaling up the technology, integrating it into the cantonal and national energy strategy and to show future scenarios of using the technology.

Work Package (WP) Tasks (T)	Partners involved in WP (those leading the WP in bold)	Start (month)	End (month)	Duration (months)
WP 1 Feasibility and economic studies	ETH/SUPSI/GES	1	48	48
Task 1.1: Pre-experiment techno-economic analysis of conceptual experimental design	ETH/SUPSI/GES	1	12	24
Task 1.2: Numerical modeling (syn-, post-experiment) of subsurface fluid/energy circulation and energy storage	ETH/SUPSI/GES	13	48	36
WP 2 Experimental design	GES/ETH	10	18	9
Task 2.1: Detailed conceptual design of experiments	GES/ETH	10	18	9
Task 2.2: Monitoring strategy	GES/ETH	13	18	6
WP 3 Experiment execution including monitoring	GES/ETH	19	48	30
Task 3.1: Single-hole experiments using hot water	GES/ETH	19	30	12
Task 3.2: Cross-hole circulation using hot water	GES/ETH	28	48	21
WP 4 Roll-out and integration in energy strategy	SUPSI/ETH/AET/GES	25	48	24
Task 4.1: Economic models and energy dispatching	SUPSI/ETH/AET/GES	31	48	18
Task 4.2: Roll-out and dissemination of technology on the cantonal and national level	SUPSI/ETH/AET/GES	31	48	18
		Start	End	Duration
Total:		1	48	48

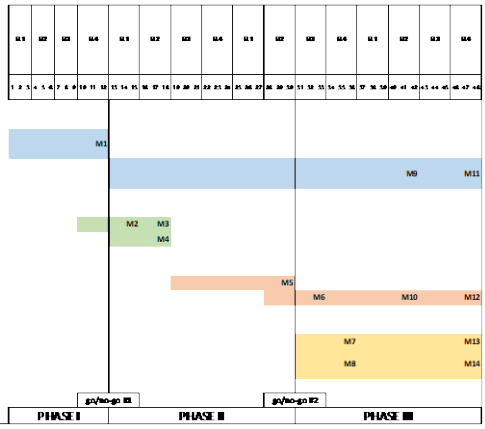

Figure 2 Organizational structure of the BEACH project with four work packages running over three phases

In this report, we will focus on the outcomes of Phase I. The overall objective in Phase I is to demonstrate the technical and economic feasibility of heat storage in fractured rocks with near real-scale tests and to find the optimal design for future scenarios at other sites and greater depths. Various storage and extraction scenarios are numerically simulated, and an experimental design is presented. The main research question is 'What are optimal reservoir and operational parameters for storing and extracting heat from fractured rocks in an economically viable way?'.

This phase concludes with a go/no-go decision. The three criteria to be fulfilled for a go decision are listed below, and they are addressed in the report in the respective subchapters.

1. Models with physically realistic model parameters should show that it is possible to store and retrieve heat from the BedrettoLab reservoir. Furthermore, it should be demonstrated that the efficiency is larger than 70%, which would make the concept economically viable. This is presented in Chapter 7.6.
2. Specific FTES use cases, other than Bedretto, should be presented, and their techno-economic properties need to be defined. In particular, the following points should be addressed.
    a. Identify use cases (producers/sources & consumers/sinks), relevant in terms of size, storage ability/need, consumers, as well as multiplication potential in Switzerland; e.g. waste incineration plants, district heating grids, industrial processes
    b. Define the requirements of a storage system for these use cases: required heat & mass flows, temperature levels, cost structures (CAPEX/OPEX), operation concept, etc.
    c. Determine the required properties (geometric, hydraulic, thermodynamic, etc.) of an underground heat storage site to fulfill these boundary conditions
    d. Assess if and how it is physically (and practically) possible to generate an FTES to meet these requirements.

    This is presented in Chapter 2.4 and 7
3. Based on the results of the previous studies, a technically and logistically feasible experimental layout should be presented, which will be employed in the next phase of the project. This is presented in Chapter 2.5

2 Approach, method, results and discussion

Most of the proposed BEACH operations are planned to be conducted in the BedrettoLab (www.bedrettolab.ethz.ch), which is an open, international research platform operated by ETH Zurich. Deep underground Laboratories, such as the BedrettoLab, bridge the gap between realistic scales (kilometer and above) and the research-lab scale (centi- or decimeter). In a natural and realistic setting, tests at the scale of tens to hundreds of meters can be conducted under controlled and repeatable conditions. The BedrettoLab provides testbeds for pure and applied research for geosciences and geoenergy, and it offers access to a wide and diverse range of research infrastructures, whereby the reservoir volume is of particular interest to the BEACH project.

2.1 Pre-knowledge on the Bedretto reservoir

The BedrettoLab provides existing infrastructure and data in fractured granite. The setup includes an injection borehole (shown in orange in Figure 3) that is subdivided in 14 intervals by a sophisticated multi-packer system. Furthermore, an extraction borehole (shown in magenta in Figure 3) was drilled

into the Bedretto reservoir. These two boreholes are surrounded by a “monitoring umbrella” including 7 additional boreholes. In these boreholes, a plethora of sensors, measuring seismicity, temperature, pressure and strain, were grouted in (Figure 4). This monitoring system is augmented by various other sensors located in the main tunnel.

The database existing for that reservoir is based on various projects run prior to BEACH: the project VALTER (Validating of Technologies for Reservoir Engineering) (Giardini et al., 2022), the two European projects ZoDrEx (Zonal Isolation, Drilling and Exploitation of EGS projects) (Meier and Christe, 2023) and DESTRESS (Demonstration of soft stimulation treatments of geothermal reservoirs) (Huenges et al., 2020) and the MISS project (Mitigating Induced Seismicity for Successful Geo-Resources Applications).

The datasets used for the BEACH model calibration are based on a detailed analysis of the hydraulic stimulation experiments conducted in the BedrettoLab. The experiments tested multiple intervals in the crystalline rock volume, densely instrumented with sensors for monitoring thermo-hydro-mechanical responses. The resulting datasets now include information on hydraulic connectivity, pressure compartmentalization, the creation of new hydraulic connections between adjacent intervals and the resulting changes in reservoir transmissivity.

The data, including hydraulic, seismic, and geomechanical observations, are comprehensively summarized in Obermann et al. (2024), Gholizadeh Doonechaly et al. (2023) and Gholizadeh Doonechaly et al (2024), providing the basis for the calibration and validation of the BEACH model.

2.1.1. Selection of borehole and interval for experiments

Figure 3 displays the configuration of boreholes in the BedrettoLab. Amongst them, ST1 is the longest (404m long) and is equipped with a multi-packer system that isolates 14 injection intervals. In each interval (except interval 10, in which sensors are damaged), the pressure and temperature can be measured in situ. ST1 diameter is 8.5”, which corresponds to a borehole size for industrial application.

Prior to the installation of the multi-packer system, ST1 was characterized to identify fractures and geological discontinuities along the borehole. Here we focus on acoustic (ATV) and optical televiewer (OTV) logs. Broadly speaking, the characterized rock volume consists of weakly foliated Rotondo granite intersected by strongly foliated ductile shear zones and brittle fracture zones (Castilla et al., 2021; Hertrich et al., 2021; Wenning et al., 2022; Ma et al., 2022). The majority of intersected structures strike NE-SW (perpendicular to the Bedretto Tunnel) to E-W and are steeply dipping (>50°), which agrees with mapping of structures along the walls of the Bedretto Tunnel (Lützenkirchen and Löw, 2011; Rast et al., 2022; Bröker et al., 2024). Figure 4 displays the integrated geophysical logs along the shallow part of ST1.

The so-called VALTER intervals (7 to 14) were stimulated following the standard protocol of pressure-controlled conditions described in Bröker et al. (2024). An example of such a protocol is provided in Figure 5, and a summary of pre- and post-stimulation transmissive capabilities is presented in Table 1.

The following criteria are considered for the selection of the target interval:

- Complexity of the fracture network: intervals intersecting many fractures are discarded. Recovering injected hot fluid is more efficient from a single fracture system because: (1) in a densely fractured volume, the fluid is distributed across numerous fractures with varying permeabilities and distinct flow paths, resulting in a more diffuse and slower recovery. In contrast, a single, highly transmissive fracture provides a direct, well-defined flow path for efficient fluid recovery; (2) in a fracture network, fluid temperature is affected by mixing of fluids from various fractures

that are not at the same temperature, thus leading to thermal dilution of the produced fluid and potential entrapment of the injected hot fluid caused by gravity effects; (3) the risk of breakthrough risk is very small, as the permeability of the surrounding granite is significantly lower than that of non-filled fractures.

- Depth: heat losses along the tubing increase with length, and therefore, with depth. In addition, the loss of injected energy eventually backflowing to the borehole from the granite also increases with depth. As such, the interval should be chosen as shallow as possible.
- Interval length: longer intervals, thus involving larger water volumes, require more time to get to the target injection temperature.
- Low seismicity: low microseismic activity during injection is required to not interfere with other on-going experiments at the BedrettoLab.
- Jacking pressure: injection will take place under controlled pressure conditions to keep downhole pressure slightly above the jacking pressure, above which seismicity starts to develop significantly. Since injected flow rate (and therefore power) increases with the imposed pressure for any given transmissivity, the jacking pressure should be as high as possible. Except interval 14 (shallowest), all jacking pressures are similar (Table 1).
- Transmissivity: the transmissivity of the target fracture should be as high as possible to maximize the extent of the injected heat plume, i.e., the area of the engineered heat exchanger.

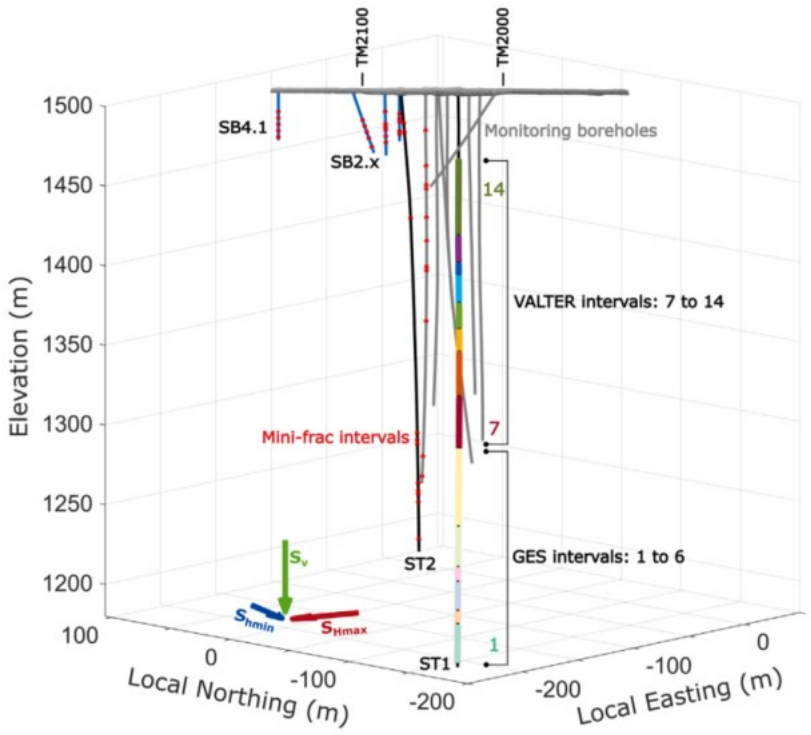

Figure 3. Stimulation (ST), monitoring (in grey) and stress measurement (SB) boreholes in the Bedretto Geothermal Testbed. The 14 stimulation intervals along ST1 are coloured. From Bröker et al. (2024).

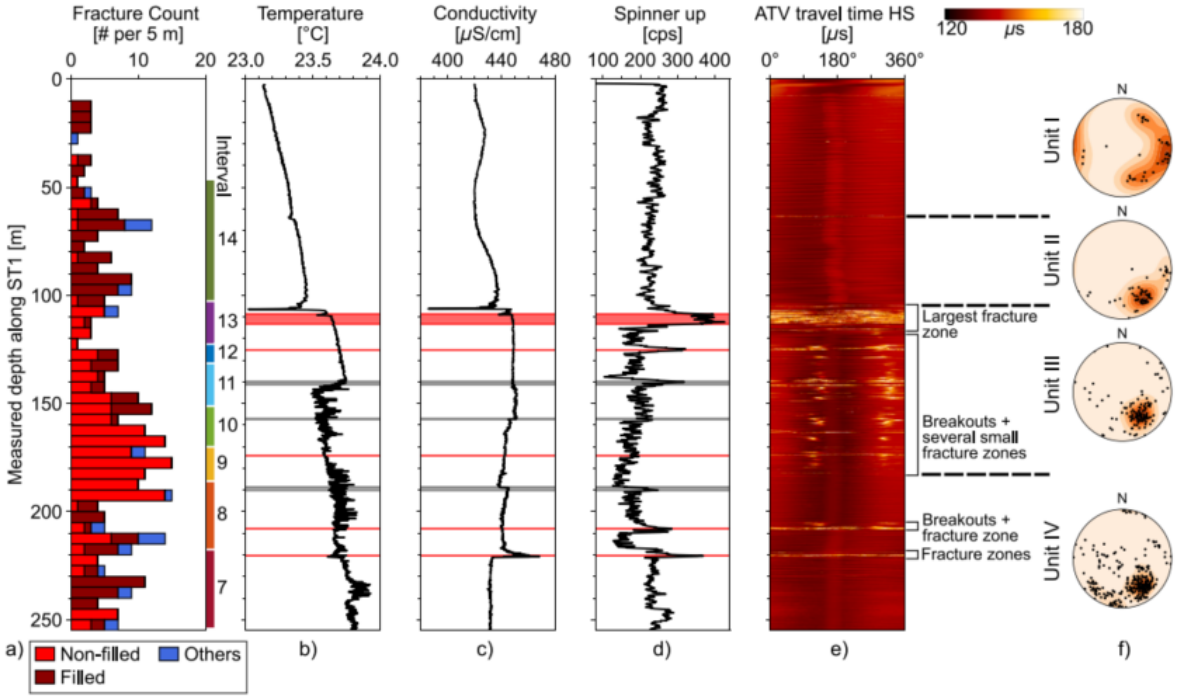

Figure 4. Integrated geophysical logs along the shallow part of ST1 (GES intervals 1 to 6 are not shown): (a) distribution of structures mapped from televiewer logs together with the extent of the stimulation intervals, (b) temperature, (c) conductivity, (d) spinner, (e) acoustic televiewer travel time (oriented to high side), (f) lower hemisphere pole plots with density contours of geological discontinuities. Fracture zones with widths greater than 10 cm are shown as red bands, and other identified inflow zones are shown as gray bands. The true aperture of fracture zones is shown. From Bröker et al. (2024).

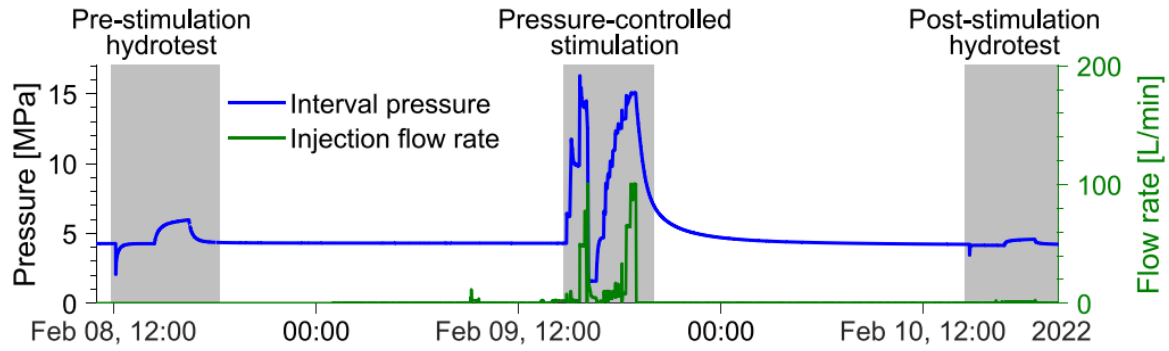

Figure 5. Injection protocol for Interval 8 consisting of a pre- and post-hydrotest to estimate the transmissivity changes due to the hydraulic stimulation. From Bröker et al. (2024).

Table 1. Overview of the key measurements from the hydraulic stimulation experiments, sorted by interval. Modified from Bröker et al. (2024).

Interval	*Depth range (mMD)*	*Length (m)*	*T pre-stimulation (m^2/s)*	*T post-stimulation (m^2/s)*	*Number of events during stimulation*	*Mean jacking pressure (MPa)*	*Comment*
7	*218.3–253.3*	*35.1*	*3.00E-07*	*2.30E-07*	*254*	*11*	*Discarded. Too deep. Too long interval*
8	*186.7–216.8*	*30.1*	*3.30E-08*	*2.30E-07*	*1289*	*13.4*	*Discarded. Too deep and intense microseismic activity. Too long interval*
9	*170.8–185.2*	*14.4*	*4.10E-08*	*2.30E-08*	*567*	*13.7*	*Discarded. Too deep and medium microseismic activity*
10	*152.0–169.3*	*17.3*	*1.80E-08*	*1.50E-08*	*611*	*12.5*	*Discarded. Deep, low transmissivity and medium microseismic activity*
11	*132.2–150.5*	*18.3*	*5.60E-08*	*4.00E-08*	*98*	*14.3*	*Selected. Intermediate depth, medium transmissivity and low microseismic activity*
12	*123.2–130.7*	*7.5*	*1.90E-08*	*1.20E-08*	*233*	*–*	*Discarded. Low transmissivity*
13	*103.4–121.7*	*18.2*	*8.40E-07*	*8.40E-07*	*2417*	*–*	*Discarded. Highest transmissivity but largest microseismic activity. Intersects the "FMZ".*
14	*47.2–101.9*	*54.8*	*2.30E-09*	*5.60E-08*	*204*	*9.9*	*Discarded. Lowest transmissivity and largest length*

Intervals 7 to 10 were discarded observing the depth criterion. Intervals 12 and 14 were discarded observing their low transmissivities and their proximity to Interval 13. Interval 13 is the one with highest

transmissivity, but also with most intense microseismic activity. In addition, the intersected Main Fault Zone (MFZ) intersects the gallery. Finally, Interval 11 has been selected as target for the first experiment after balancing all the aforementioned criteria.

2.1.2. More detailed description of Interval 11

Interval 11 isolates the depth segment 132.2–150.5 along ST1. Multiple non-filled fractures and two fracture zones exist, with orientation 233°/58°. Just above the fracture zone at 142 m MD, an increase of fluid temperature and inflow in the spinner log is observed (Figure 4b and d), which reveals the presence of a conductive feature suitable for heat storage. Figure 6 displays a zoom of the ATV log along interval 11.

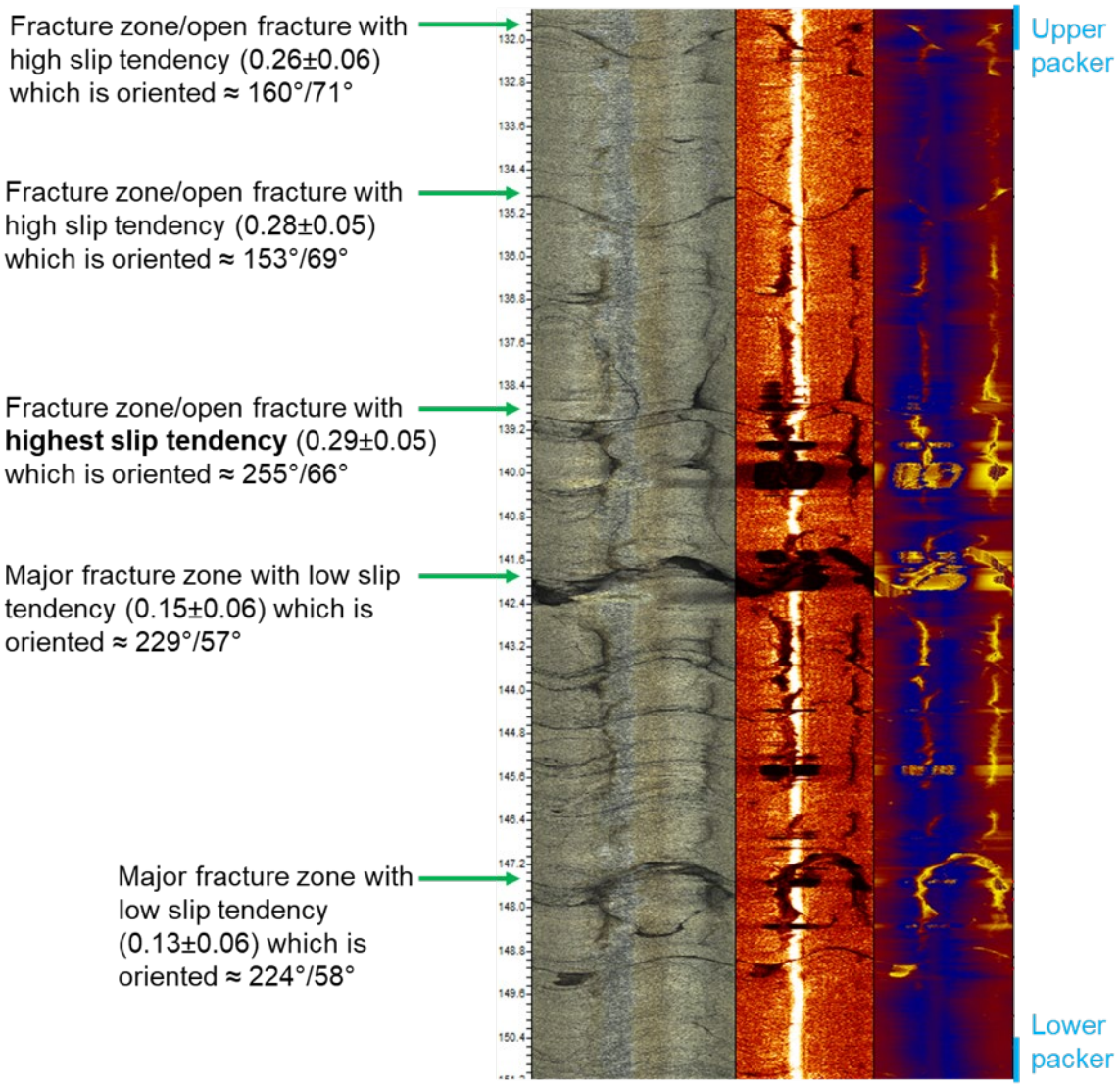

Figure 6. Zoom of ATV log at Interval 11.

The static pressure at Interval 11 is 3.6 MPa (third lowest along ST1). Initial transmissivity was 5.6E-08 m^2/s. In March 2022, 2190 L of water were injected and 189 L back-flew to the borehole after re-opening (17% of the injected volume). During injection, the highest injection pressure was 17.5 MPa, with a

maximum injection flow rate of 9.8 L/min. In July 2023, it was re-stimulated with a volume of 6250 L under controlled flow rate conditions (Figure 7). Notably, transmissivity decreased slightly after stimulation, which is attributed to partial closure of the fracture after the final shut-in.

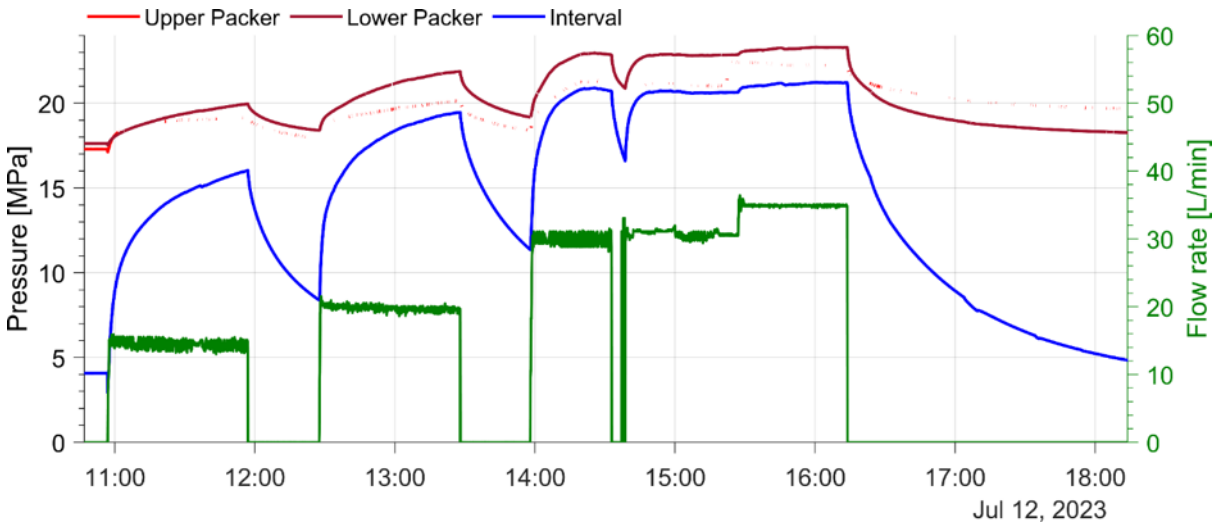

Figure 7. Temporal evolution of packer and interval 11 downhole pressure, and injection flow rate. Re-stimulation under controlled flow rate conditions.

Obermann et al. (2024) shows the spatial distribution of induced microseismic events associated with the most recent stimulation of interval 11. The data indicates that interval 11 intersects a substantial, highly transmissive structure, suggesting it as a strong candidate for a FTES system. Despite enhanced connectivity of fractures (i.e., a strongly fractured rock volume) would lead to a larger surface of the heat exchanger, the yield of the FTES mostly depends on the amount of hot fluid recovered, which is hindered by the complexity of the fracture network. It is worth noting that the first experiment in Bedretto serves as demonstrator of the technical feasibility of heat injection and extraction in/from a fractured rock. Further experiments may include the use of all intervals along ST1, making the experiment closer to a real-world scenario. In fact, the efficiency of the base case scenario (section 2.4.3) has been evaluated using all intervals of ST1.

2.2 Pre-knowledge on real case scenarios

A large part of the Swiss underground is made of fractured crystalline rocks. This shows the wide applicability of the new technology FTES. Therefore, real case scenarios can be realized in various parts of Switzerland.

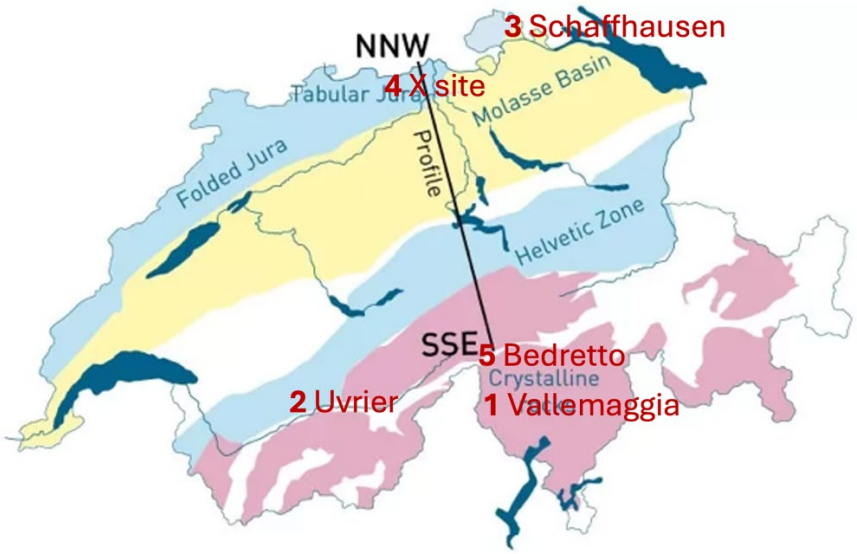

Figure 8 Map of Switzerland with simplified geology: Jura with limestones, Molasse Basin with mountain deposits, Helvetic Zone with marl-rich sediments and crystalline rocks of the Alps. Profile not shown here.

Roughly 60% of Switzerland consists of fractured rocks: Jura, Helvetic Zone, the Alps and even the deeper Molasse Basin. Several real-case scenarios were selected during the first Phase of BEACH, which are all located in fractured rocks (Figure 8): the Vallemaggia, Uvrier, Schaffhausen, and an existing industrial area in northern Switzerland (termed here X for confidentiality). All cases represent different stages of possible project development as shown in Figure 9. The Vallemaggia and Uvrier case are representative cases for the reconnaissance phase, where geological fieldwork is conducted or first surface studies on available infrastructure are carried out. The Schaffhausen case represents the drilling phase, we assume boreholes have been drilled and can be used for injection and production of hot water. The X case is the most developed case study, where we assume an FTES to be in operation already.

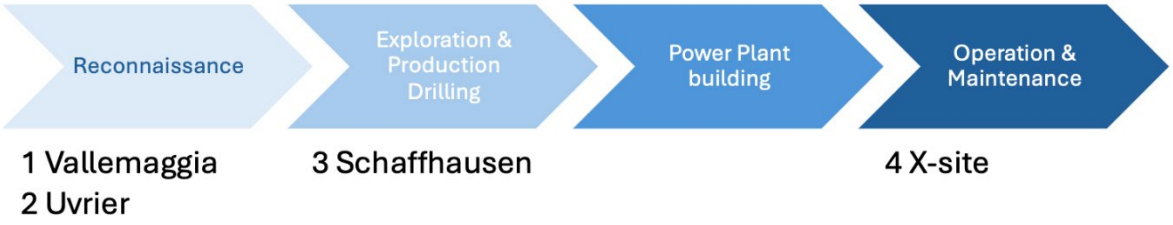

*Figure 9 Project development phases for FTES systems, including the four case studies across Switzerland investigated in this report (see Section **Fehler! Verweisquelle konnte nicht gefunden werden.**)*

We conducted a detailed study on outcrops in **Vallemaggia** as a representative exploration study in a green field, which would be conducted in an area where a heat storage plant would be built (Location 1, Figure 10). The focus of this study was on the subsurface.
Another possible site where a heat storage plant could be built is located at **Uvrier** (Location 2, Figure 10), where already a waste incineration plant is located, which produces excess heat. Additionally, in that area, crystalline rock is present at the surface, hot springs are present and deep boreholes have been drilled formerly, which contribute to a better understanding of the subsurface.
The **Schaffhausen** area (Location 3, Figure 10) appears suitable for deploying an FTES in future. This location offers several advantages, including the presence of crystalline rock formations at shallow depth, favourable surface condition, and proximity to industrial heat sources.
The **X site** selection is based on a starting industry collaboration with operators of the industrial area. For this location we defined the requirements for a storage system for this use case with heat and mass flows, temperatures and costs. At site X, the geology and surface conditions are especially promising because a fractured granite is located only 300 m below surface only. At the location, industry waste heat is available at 150-200°C as steam, which is currently dissipated in the air. We conducted a techno-economic feasibility study for that site.
The most detailed numerical studies of a FTES system were conducted for the **Bedretto** case (Location 5, Figure 10), where also the experiments will take place.
All studies on the single locations are presented in Section **Fehler! Verweisquelle konnte nicht gefunden werden.**. After this introduction to the setting in Switzerland a generic use case is presented using knowledge from all site studies showing the economic feasibility of FTES setups.

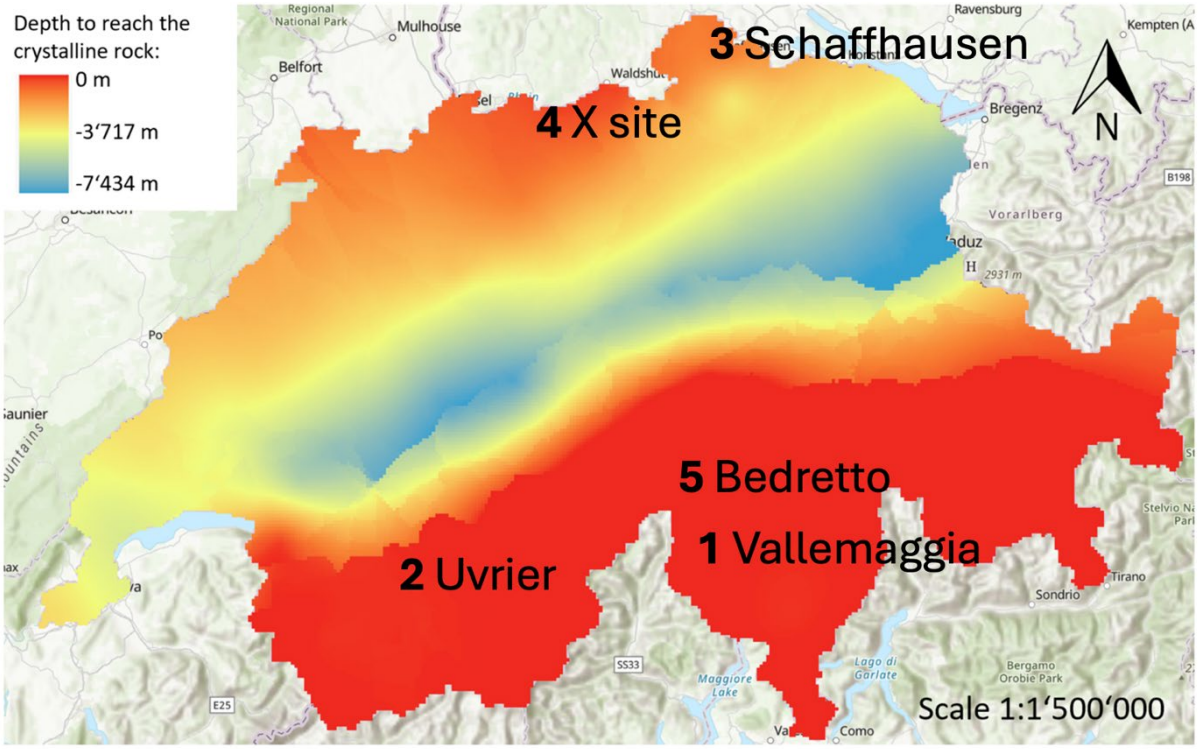

Figure 10 Map of Switzerland with extrapolation of the depth to the crystalline rock made in ArcGIS Pro with the "Empirical Bayesian Kriging"- tool and with 4 real case scenario locations studied in BEACH Phase I. 1: Vallemaggia, 2:Uvrier, 3: Schaffhausen, 4: X, 5: Bedretto (modified after Merkofer et al., 2024)

2.3 FTES use case at real-scale sites in Switzerland

In a first step, we made an overall assessment of heat producers and critical FTES properties in Switzerland. Then, we present a generic use case for building FTES in Switzerland.

2.3.1. FTES use cases in Switzerland - overview

In order to show that it is possible to store heat in an FTES in a way that allows for a viable real-life operation, different use cases were evaluated for Switzerland. In a first step, waste incineration plants, which are possible sources/producers of heat, were mapped against possible users of heat, as head demand for homes (Figure 11). Heat production and demand are expectedly high in Northern Switzerland near the agglomeration zones, but also in the main valleys of Southern Switzerland. Additionally, the alpine crystalline rocks are a possible target formation and mapped in Figure 10.

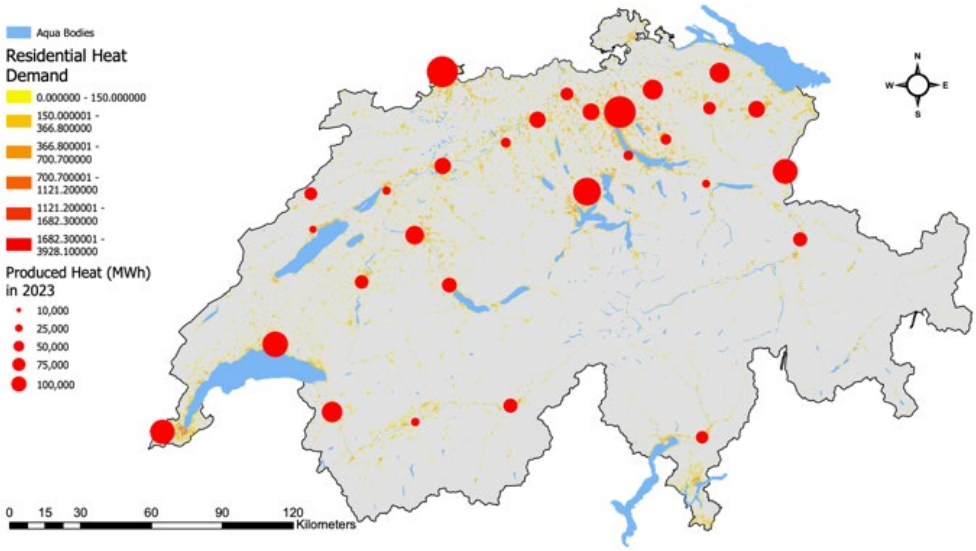

Figure 11 Map of Switzerland showing the heat sources in MWh from incineration power plants as red circles and the residential heat demand as population density. The map is based on data from the Geoinformationsplattform der Schweizerischen Eidgenossenschaft (geo.admin.ch). The heat production data for 2023 were sourced from energy output records of incineration power plants, while residential heat demand was derived from demographic heat demand layers. Data were processed using GIS analysis and aggregated within administrative boundaries.

In a next step the depth to a target temperature of 60°C was mapped for the whole the country (Figure 12). The target temperature was chosen based on the most probable excess heat that is accessible from industrial processes. Also, lower temperatures might be available. If storing water in these temperature ranges in reservoirs of similar temperature, the storage plant will not experience heat loss during storage periods. However, if the target temperature is at greater depth, which would cause higher drilling costs and lower permeabilities, one might consider a low-temperature reservoir and accept heat loss instead of higher drilling risks. 60°C target temperature was chosen as the good balance between heat loss during storage and drilling depth/costs. Though, the most important factor is always the depth to crystalline fractured rock.

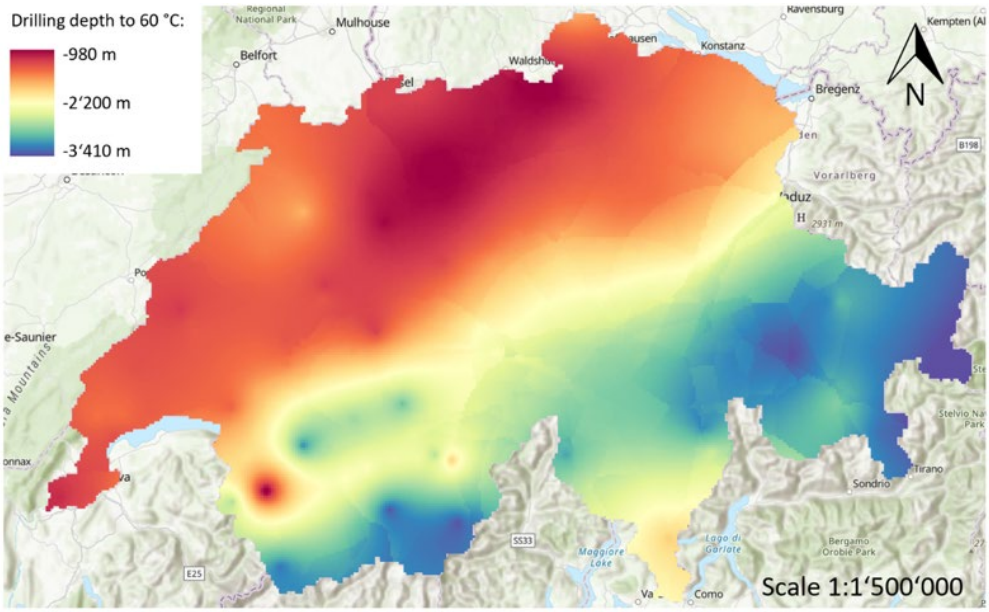

Figure 12 Map of Switzerland showing the depth to the target temperature of 60°C (modified after Merkofer et al., 2024, see also Appendix 6.2)

2.4 Generic use case

To evaluate the FTES potential in Switzerland, we built a synthetic reservoir model based the data from the studies discussed in the previous sections. Specifically:

- Fracture properties from Bedretto and Vallemaggia
- Depth/basement information from Schaffhausen
- Surface information from Uvrier

We assumed a sector model with size of 410x410x300 m3 domain, discretized into 41x41x30 grids with a uniform grid size. The depth of reservoir top is 500m. For horizontal direction, open outer boundaries (constant pressure) are applied, whereas the overburden and underburden are assumed in vertical directions. A multiple-continuum modelling approach (dual-porosity single-permeability) approach is employed to capture multi-scale flow effects in the rock matrix and small fractures. Summary of the base case reservoir properties are provided in Table 2. The base operational parameters follow **Fehler! Verweisquelle konnte nicht gefunden werden.** (the Schaffhausen case study).

Table 2 Summary of the base case reservoir properties

Parameter	Value	unit
Matrix porosity	0.001	-
Matrix permeability	0.0032	mD
Fracture porosity	0.1	-
Fracture permeability	10.0	mD

Permeability anisotropy (kv/kh)	0.4	-
Shape factor (fracture spacing)	1.0	m^{-2}
Rock compressibility	1.49e-7	kPa^{-1}
Rock heat capacity (target reservoir)	2.13e6	$J/(m^3\text{-}^oC)$
Rock thermal conductivity (target reservoir)	2.59e5	J/(m-day-^{o}C)
Rock heat capacity (surrounding formation) *	2.13e6	$J/(m^3\text{-}^oC)$
Rock thermal conductivity (surrounding formation) *	2.59e5	J/(m-day-^{o}C)
Initial reservoir temperature	Figure 13	^{o}C
Initial reservoir pressure	Figure 13	kPa

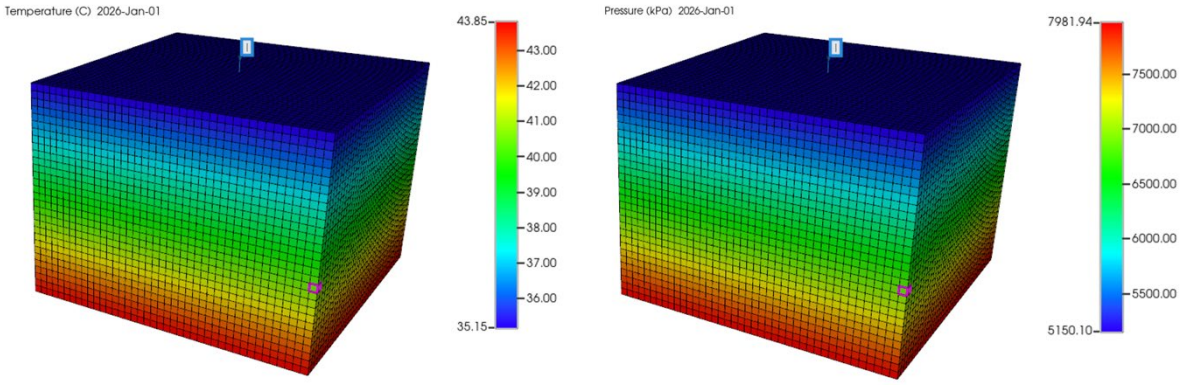

Figure 13 Initial reservoir conditions: temperature (left) and pressure (right)

To evaluate FTES performance under uncertainty, we followed a Design of Experiment (DoE) approach (Bhark et al., 2014), consisting of:

1. Identification of potentially influential parameters during FTES
2. Parameter screening via sensitivity analysis
3. Sampling from identified influential parameters
4. Forecasting using representative model(s)

2.4.1. Identification of potentially influential parameters

Based on the previous sections, uncertain subsurface parameters and their ranges were identified. (Table 3).

Table 3 Summary of the uncertain parameters and their ranges

Parameter	Symbol	Low	Midrange	High
Matrix porosity, (-)	POR_M	0.0005	0.001	0.0015
Matrix permeability, (mD)*	PERM_M	-3	-2.5	-2
Fracture porosity, (-)	POR_F	0.05	0.1	0.15
Fracture permeability, (mD)*	PERM_F	0.5	1.0	1.5
Permeability anisotropy (-)	KVKH	0.2	0.4	0.6
Shape factor (m^{-2})	SIGMAMF	0.3	1.0	1.7

*log10 scale

2.4.2. Parameter screening via sensitivity analysis.

A one-variable-at-a-time (OVAT) approach was used to generate a tornado plot (Figure 14) to assess parameter sensitivity. OVAT is simple but has limitations, such as ignoring interactions between parameters and potential nonlinearities, and this could be problematic when the problem is highly non-linear. However, given that FTES involves relatively simple dynamics (single-phase water and a single well), OVAT is sufficient.

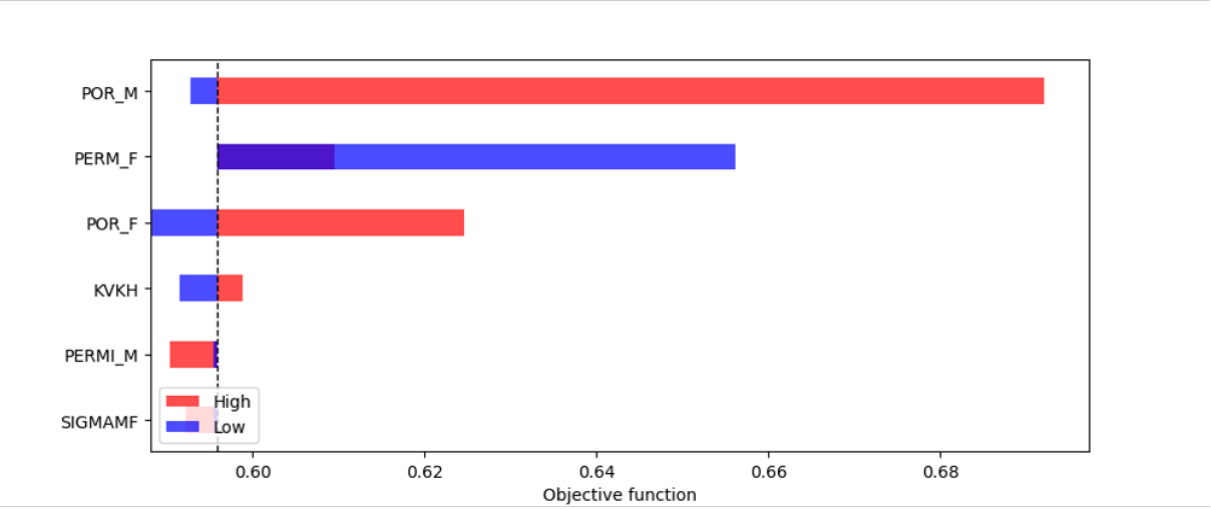

Figure 14 Tornado plot of FTES sensitivity (Objective function: thermal recovery efficiency). The parameter names correspond to Symbol in Table 7.

As a result, we have identified three most influential parameters constituting FTES efficiency: matrix porosity, fracture permeability, and fracture porosity.

2.4.3. Sampling from identified influential parameters

Using Latin Hypercube Sampling (LHS) (Helton & Freddie, 2003), we generated 50 samples varying the three key parameters. The FTES simulations were run using CMG STARS, with results summarized in Figure 15.

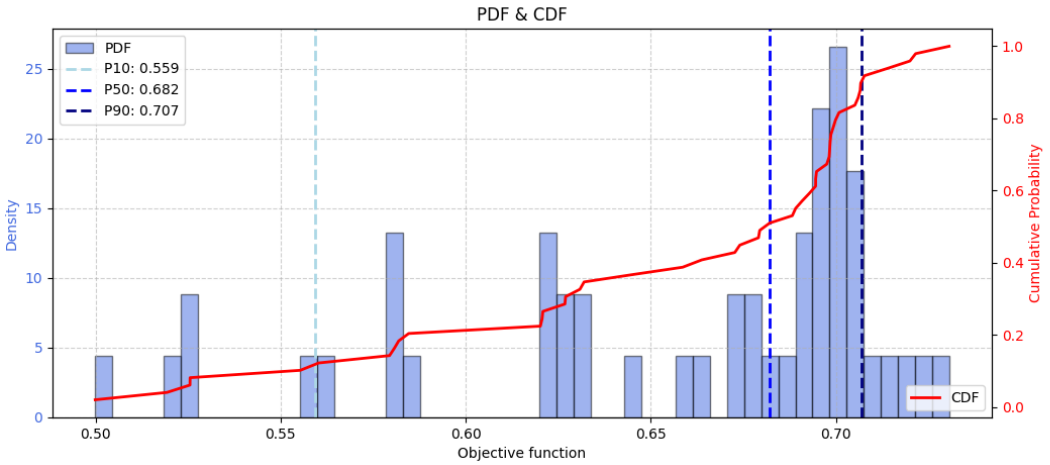

Figure 15 FTES simulation results: probability distribution function (PDF) and cumulative distribution function (CDF) of thermal recovery efficiency.

The key observations:

- The histogram (PDF) and the steep increase in the CDF curve show that most of the values of thermal recovery efficiency are clustered around 0.68-0.71, with a peak density near 0.70.
- The P50 efficiency is 0.682, meaning that 50% of cases exceed this value.
- We simulated 5 cycles (5 years) only. Simulating longer period of time would increase the efficiency.

Additionally, the values of the key parameters at P10, P50, and P90 are summarized below. The results are consistent with the tornado chart (Figure 14).

Table 4 Summary of the representative models. The parameter names correspond to Symbol in Table 7.

Representative sample	POR_M (-)	PERM_F (mD)	POR_F (-)	Efficiency (-)
P10	0.0019	21.49	0.015	0.56
P50	0.0014	4.74	0.043	0.68
P90	0.0009	11.56	0.046	0.71

2.4.4. Forecasting using representative model(s)

The P50 model was selected as a representative model to analyse the sensitivity of injection fluid temperature. Three cases with 40, 60, and 80 degrees were investigated (Table 5).

Table 5 Summary of the operational parameters

Parameter	Value	unit
Maximum injection BHP	9,000.0	kPa

Injection/production rate	120	L/min
Injection fluid temperature	40, 60, 80	°C
Minimum production BHP	4000.0	kPa

The simulation results are summarized below. In Figure 28, the water rate and temperature are recorded only when the well is operating—either injecting or producing. During shut-in (rest) periods, these values are not recorded, which is why they appear as zero during those intervals.

Table 6 Simulation results

Scenario	Injection fluid temperature (deg. C)	Efficiency (-)
Case 1	40.0	0.93
Case 2	60.0	0.70
Case 3	80.0	0.68

Key observations:

- Case 1 (40 deg. C) with lower injection temperature showed higher efficiency. This is because the bottom part of the reservoir has an initial temperature higher than the injection temperature.
- Case 3 (deg. 80) had slightly lower efficiency than case 2 (deg. 60). This is primarily because the higher temperature reduced viscosity, and increased mobility, allowing for higher injection volume with the same max bottom-hole pressure (BHP) constraint (Figure 16). This resulted in slightly lower thermal recovery.

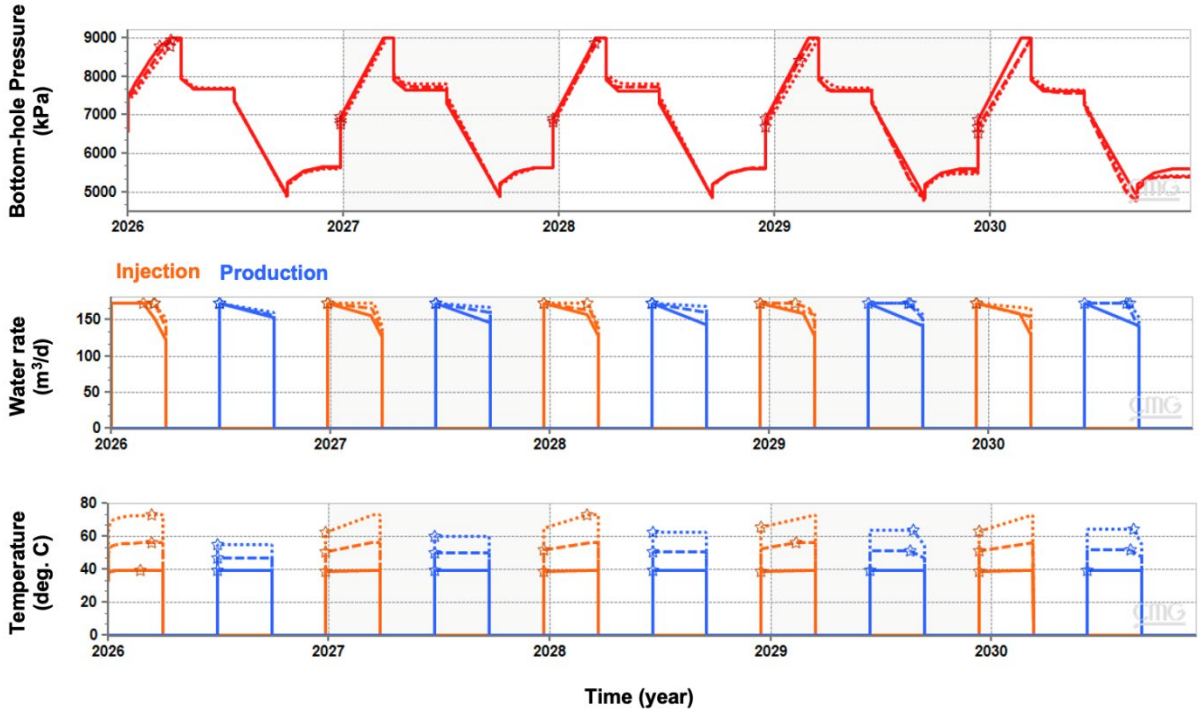

Figure 16 Summary of FTES simulation results using P50 parameters with varying injection temperature. (solid line: case 1, dashed line: case 2, and dotted line: case 3)

2.4.5. Sensitivity to lower reservoir temperatures

To explore the sensitivity of the results on the choice of reservoir temperature, we computed models with reservoir temperatures at 500 m depth of 25°C and 15°C (Figure 17), for which heat losses are expected to be higher and the efficiency to be lower. To this end, we also extended the numbers of modelled cycles to explore how the efficiency develops in the long term (i.e. up to 20 years).

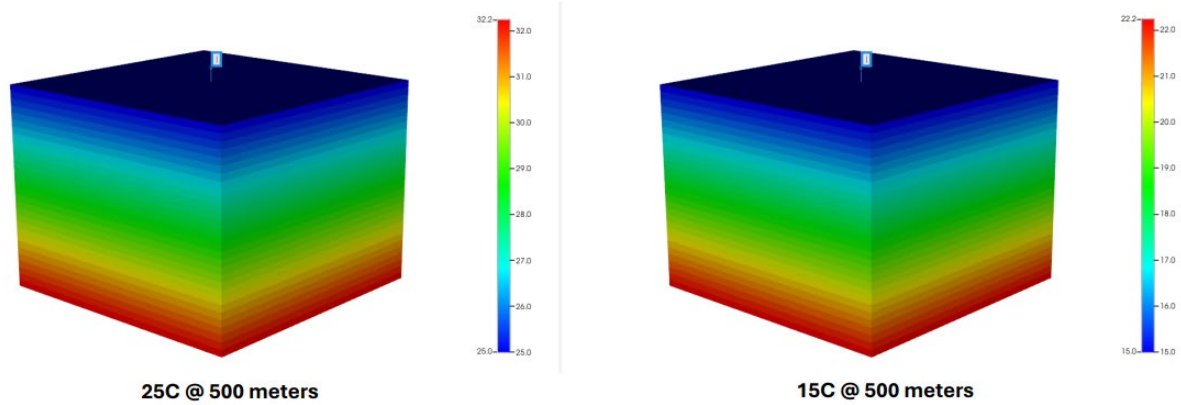

Figure 17: Initial reservoir temperature of two alternative with lower temperature, i.e. 25°C and 15°C

The resulting efficiency development over time is shown in Figure 18. In the early cycles of operation, a larger fraction of the injected water's energy is stored in the surrounding rock, resulting in lower recovery efficiencies. However, this heat loss leads to a gradual temperature increase near the wellbore. As a result, less heat is stored per unit of heat recovered in subsequent cycles, leading to an increase in thermal recovery efficiency over time. The rate of this increase slows as the rock temperature approaches the injection temperature.

A difference in reservoir temperature (15 °C vs. 25 °C at 500 meters depth) leads to a 5–10%variation in thermal recovery efficiency.

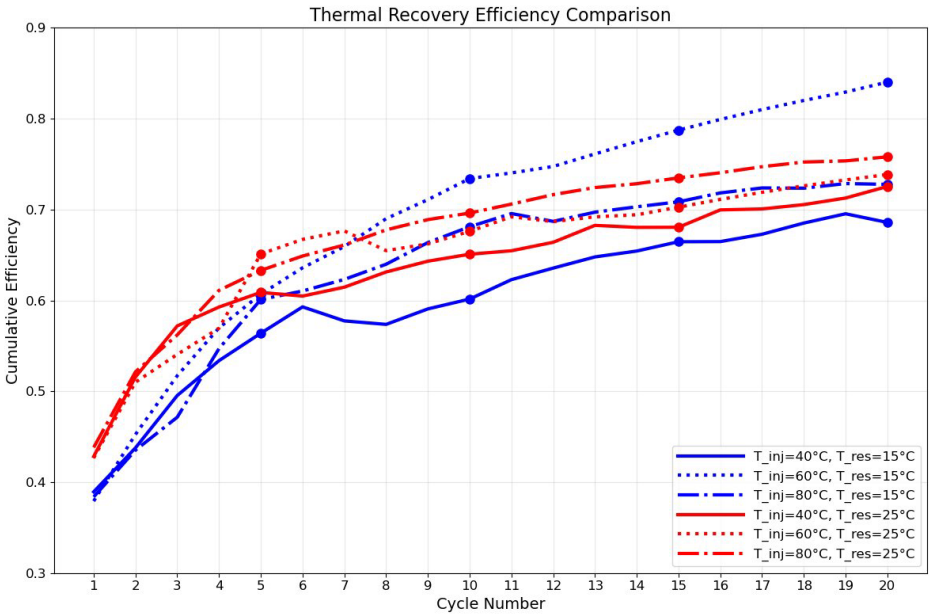

Figure 18: Evolution of efficiency for different scenarios regarding injection temperature and reservoir temperature.

2.4.6.Summary of reservoir modelling

- We built a generic model using the available data in Switzerland from the previous sections.
- We conducted a Design of Experiment (DoE) analysis to identify key parameters influencing FTES performance, generated 50 realizations, and simulated FTES performances.
- Based on the P50 representative case, we simulated five operational cycles (5 years) with varying injection fluid temperatures and found that a thermal recovery efficiency of over 70% is achievable.
- Analysis of the probability distribution function PDF and CDF shows that the majority of cases exhibit efficiencies around 0.70.
- Thermal recovery efficiency generally improves with extended operation.
- Even for lower reservoir temperatures efficiencies of 0.7 can be reached after more than 10 cycles.
- Generally, FTES operations could be further optimized through parameter tuning, such as adjusting injection temperature, flow rates, and cycle durations, to maximize efficiency.

The economic viability is discussed in the next section.

2.4.7.Techno-economic study on FTES

We outlined the key assumptions and methodologies used in the economic evaluation of FTES. The analysis primarily focuses on financial viability, energy pricing, and cost estimations based on available data from the provided dataset.

Table 7 Key Economic Assumptions for the Base case study "Schaffhausen"

Parameter	Value	Unit
Thermal Energy Selling Price for district heating	0.15	CHF/kWh
Feed-In Tariff:	0.12	CHF/kWh
Grid Electricity Price	0.01*	CHF/kWh
Project Lifetime	30	year
Discount Rate	5%	percentage
Contingency Cost percentage	5%	percentage
Gov. contribution	0%	percentage
mass flow rate	2	kg/s
current fluid temperature	40	C
Target temperature	60	C
purchase rate hot fluid from industry per kg	0	CHF/kg
Specific Heat of Water	4.186	kJ/(kg·°C)
Operating Hours during summer	10	hours
Operating Hours during winter	10	hours
injected (produced) mas	6'480'000.00	kg
Seasonal periods	90	days
Insulation pipe length	100	meter
Insulation pipe cost including installation	65	CHF/meter

* We assume that the electricity to heat up the fluid during the summer is almost for free (or in other word, the industrial complex are providing the fluid hot at 60C).

Table 8 NoloClimat Boiler Unit specification

Parameter	Value	Unit
max flow rate	0.67	kg/s
Power consumption per unit	80	kW
Purchase Cost per unit	10783	CHF

Services fee	5000	CHF
Boiler Efficiency	90%	percentage

Table 9 Cost Considerations

NoloClimat Boiler Capacity for thermal Power (kW = kJ/s)		
Temperature increase	20	C
Required Energy to heat 1 kg H2O	83.72	kJ/kg
Required thermal Power at flowrate	167.44	kW
Number of Boiler Units Needed	3	#
Boiler Capacity for thermal Power (current rate)	186.04	kW
Boiler Capacity for thermal Power (full capacity)	265.34	kW
Total energy over 90 days	167'440.00	kWh
Total Cost for thermal power	1'674.40	CHF/90days

Energy consumption and cost of operating the pump over 90 days		
High-pressure Triplex plunger pump k4500-3		
Pump power consumption	22.5	kw
Total Energy Consumption over 90 days	20250	kWh
Total Cost for the pumping power	202.50	CHF/90days

Drilling well(s)		
depth	555	meter
no of well	1	
drilling cost rate	1'000.00	CHF/meter
drilling completion rate	500.00	CHF/meter

Wellbores cost	832'500.00	CHF
Existence infrastructure		CHF
Overall-cost	0.83	MCHF

Table 10 Thermal Energy output

Parameter	Value	Unit
FTES efficiency from reservoir simulation	76%	%
Average Temperature at WellHead	45.4	C
Ambient Temperature during the winter	5	C
The energy added to each kilogram of water	169.1144	kJ/kg
Total thermal power output over 90 days	1'095'861'312.00	kJ
Total thermal Energy	304'405.92	kWh

2.4.8. Financial aspects

Table 11 CAPEX

Boiler Purchase	37'188.06	CHF
High-pressure Triplex plunger pump k4500-3	85'000.00	CHF
Borehole drilling completion	832'500.00	CHF
insulation piping	6'500.00	CHF
Auxiliary Systems: control systems, instrumentation	10000	CHF
Contingency Cost	48'559.40	CHF
Total	**1'019'747.46**	**CHF**
Gov. Fund	-	CHF

Eff. Capex	1.02	MCHF

OPEX

regular maintenance (0.5%)	5'098.74	CHF/year
Operational Costs: Labour cost, admin, consumables	125'000.00	CHF/year
Hot-fluid purchase cost from industry	-	CHF/year
Electricity Costs for boiler	1'674.40	CHF/year
Electricity Costs for pump during winter	202.50	CHF/year
Electricity Costs for pump during summer	202.50	CHF/year
Contingency Cost	6'608.91	CHF/year
Total	**0.14**	**MCHF/year**

ANNUAL REVENUE

Annual Revenu		
Selling thermal energy over the winter	45'660.89	CHF/year
Total	**0.05**	**MCHF/year**

2.4.9. Key Assessment Parameters

- **Payback Period**

The payback period is the time required for the cumulative discounted cash flow to become positive, indicating the point at which the initial investment is recovered. It is a critical measure of project risk and financial feasibility.

- **Net Annual Cash Flow**

Net annual cash flow represents the difference between annual revenues and costs, providing an estimate of the project's profitability on a yearly basis. This parameter is crucial for assessing operational efficiency and sustainability.

- **Total NPV**

Total Net Present Value (NPV) is the sum of all discounted cash flows over the project's lifetime (i.e. the total expected value of future cash flows discounted to the present). It provides a comprehensive measure of the project's financial performance, with a positive NPV indicating overall economic viability.

Payback Period	999.00	year
Net Annual Cash Flow	-0.09	MCHF/year
Total NPV	-58.86	MCHF

Figure 19: The top figure illustrates the cumulative discounted cash flow for a mass flow rate of 2 kg/s (120 l/min), showing no economic viability as the cash flow remains negative throughout the project lifetime. In contrast, the bottom figure represents the same cash flow scenario but with a mass flow rate of 13 kg/s, while keeping all other parameters constant. The bottom scenario demonstrates economic viability with a payback period of approximately 12 years.

2.4.10. Sensitivity Analysis

We used the discount factor to adjust future cash flows to their present value. It decreases over time, reflecting the reduced value of future cash flows due to inflation, risk, and opportunity cost. Additionally, Discounted Cash Flow (DCF) has been estimated to the present value of expected future cash inflows and outflows. The sum of all DCF values over the project lifetime provides an estimate of the project's total present value NPV. Cumulative Discounted Cash Flow is the running total of the discounted cash flows over time. It provides insight into when an investment breaks even and starts generating net positive returns. The break-even point occurs when the cumulative DCF equals the initial investment.

- **STEP 01: Sensitivity analysis for massflow rate vs the no. of the well to find the best combination for the mass flowrate and no. of the wells that achieve >70% efficiency.**

Payback Period

[years]

Mass flowrate (kg/s) \ Number of well	1	2	3	4	5	6	7	8	9	10	11	12	13	14	15
1	999.00	999.00	999.00	999.00	999.00	999.00	999.00	999.00	999.00	999.00	999.00	999.00	999.00	999.00	999.00
2	999.00	999.00	999.00	999.00	999.00	999.00	999.00	999.00	999.00	999.00	999.00	999.00	999.00	999.00	999.00
3	999.00	999.00	999.00	999.00	999.00	999.00	999.00	999.00	999.00	999.00	999.00	999.00	999.00	999.00	999.00
4	999.00	999.00	999.00	999.00	29.66	25.08	22.64	21.11	20.07	19.30	18.72	18.26	17.89	17.59	17.33
5	999.00	999.00	27.27	19.47	16.65	15.17	14.27	13.65	13.21	12.87	12.61	12.40	12.22	12.07	11.95
6	999.00	999.00	16.24	13.16	11.80	11.02	10.52	10.17	9.92	9.72	9.57	9.44	9.33	9.24	9.17
7	999.00	17.64	11.77	10.02	9.19	8.69	8.37	8.13	7.96	7.83	7.73	7.64	7.57	7.51	7.45
8	999.00	12.70	9.28	8.12	7.54	7.19	6.95	6.79	6.66	6.57	6.49	6.42	6.37	6.32	6.29
9	999.00	9.99	7.69	6.84	6.41	6.14	5.96	5.83	5.73	5.66	5.60	5.55	5.51	5.47	5.44
10	25.10	8.28	6.58	5.92	5.58	5.37	5.22	5.11	5.03	4.97	4.92	4.88	4.85	4.82	4.79
11	17.08	7.08	5.76	5.23	4.94	4.77	4.65	4.56	4.49	4.44	4.40	4.36	4.33	4.31	4.29
12	13.16	6.21	5.12	4.68	4.44	4.29	4.19	4.11	4.05	4.01	3.97	3.94	3.92	3.90	3.88
13	10.79	5.54	4.63	4.25	4.03	3.90	3.82	3.75	3.70	3.66	3.63	3.60	3.58	3.56	3.55
14	9.19	5.00	4.22	3.88	3.70	3.59	3.51	3.45	3.40	3.37	3.34	3.31	3.29	3.28	3.26
15	8.04	4.57	3.88	3.59	3.42	3.32	3.24	3.19	3.15	3.11	3.09	3.07	3.05	3.03	3.02
16	7.17	4.21	3.60	3.33	3.18	3.08	3.01	2.97	2.93	2.90	2.88	2.86	2.84	2.83	2.82
17	6.49	3.91	3.36	3.11	2.97	2.88	2.82	2.78	2.74	2.72	2.70	2.68	2.66	2.65	2.64
18	5.93	3.66	3.14	2.92	2.79	2.71	2.65	2.61	2.58	2.56	2.54	2.52	2.50	2.49	2.48
19	5.49	3.44	2.96	2.75	2.63	2.56	2.51	2.47	2.44	2.41	2.39	2.38	2.36	2.35	2.34
20	5.10	3.24	2.80	2.61	2.49	2.42	2.37	2.33	2.31	2.28	2.26	2.25	2.24	2.23	2.22
21	4.78	3.07	2.66	2.47	2.37	2.30	2.25	2.22	2.19	2.17	2.15	2.13	2.12	2.11	2.10
22	4.51	2.92	2.53	2.36	2.25	2.19	2.14	2.11	2.08	2.06	2.04	2.03	2.02	2.01	2.00
23	4.27	2.78	2.42	2.25	2.15	2.09	2.04	2.01	1.99	1.97	1.95	1.94	1.93	1.92	1.91
24	4.05	2.66	2.31	2.15	2.06	2.00	1.96	1.93	1.90	1.88	1.87	1.86	1.85	1.84	1.83
25	3.87	2.56	2.22	2.06	1.97	1.92	1.88	1.85	1.83	1.81	1.79	1.78	1.77	1.76	1.75

Net Annual Cash Flow

[million CHF/year]

Mass flowrate (kg/s) \ Number of well	1	2	3	4	5	6	7	8	9	10	11	12	13	14	15
1	-0.11	-0.10	-0.08	-0.06	-0.04	-0.02	###	0.01	0.03	0.05	0.07	0.09	0.10	0.12	0.14
2	-0.09	-0.05	-0.01	0.03	0.07	0.11	0.15	0.19	0.24	0.28	0.32	0.36	0.40	0.44	0.48
3	-0.07	-0.01	0.06	0.12	0.18	0.25	0.31	0.38	0.44	0.50	0.57	0.63	0.70	0.76	0.82
4	-0.05	0.04	0.12	0.21	0.30	0.38	0.47	0.56	0.64	0.73	0.82	0.90	0.99	1.08	1.16
5	-0.03	0.08	0.19	0.30	0.41	0.52	0.63	0.74	0.85	0.96	1.07	1.18	1.29	1.40	1.51
6	-0.01	0.13	0.26	0.39	0.52	0.66	0.79	0.92	1.05	1.19	1.32	1.45	1.58	1.72	1.85
7	0.02	0.17	0.33	0.48	0.64	0.79	0.95	1.10	1.26	1.41	1.57	1.72	1.88	2.03	2.19
8	0.04	0.22	0.39	0.57	0.75	0.93	1.11	1.28	1.46	1.64	1.82	2.00	2.17	2.35	2.53
9	0.06	0.26	0.46	0.66	0.86	1.06	1.27	1.47	1.67	1.87	2.07	2.27	2.47	2.67	2.87
10	0.08	0.31	0.53	0.75	0.98	1.20	1.42	1.65	1.87	2.10	2.32	2.54	2.77	2.99	3.21
11	0.10	0.35	0.60	0.84	1.09	1.34	1.58	1.83	2.08	2.32	2.57	2.82	3.06	3.31	3.56
12	0.13	0.39	0.66	0.93	1.20	1.47	1.74	2.01	2.28	2.55	2.82	3.09	3.36	3.63	3.90
13	0.15	0.44	0.73	1.02	1.32	1.61	1.90	2.19	2.49	2.78	3.07	3.36	3.65	3.95	4.24
14	0.17	0.48	0.80	1.11	1.43	1.74	2.06	2.37	2.69	3.00	3.32	3.63	3.95	4.26	4.58
15	0.19	0.53	0.87	1.20	1.54	1.88	2.22	2.56	2.89	3.23	3.57	3.91	4.25	4.58	4.92
16	0.21	0.57	0.93	1.30	1.66	2.02	2.38	2.74	3.10	3.46	3.82	4.18	4.54	4.90	5.26
17	0.23	0.62	1.00	1.39	1.77	2.15	2.54	2.92	3.30	3.69	4.07	4.45	4.84	5.22	5.60
18	0.26	0.66	1.07	1.48	1.88	2.29	2.69	3.10	3.51	3.91	4.32	4.73	5.13	5.54	5.95
19	0.28	0.71	1.14	1.57	2.00	2.42	2.85	3.28	3.71	4.14	4.57	5.00	5.43	5.86	6.29
20	0.30	0.75	1.20	1.66	2.11	2.56	3.01	3.46	3.92	4.37	4.82	5.27	5.72	6.18	6.63
21	0.32	0.80	1.27	1.75	2.22	2.70	3.17	3.65	4.12	4.60	5.07	5.55	6.02	6.50	6.97
22	0.34	0.84	1.34	1.84	2.33	2.83	3.33	3.83	4.33	4.82	5.32	5.82	6.32	6.81	7.31
23	0.37	0.89	1.41	1.93	2.45	2.97	3.49	4.01	4.53	5.05	5.57	6.09	6.61	7.13	7.65
24	0.39	0.93	1.47	2.02	2.56	3.10	3.65	4.19	4.73	5.28	5.82	6.36	6.91	7.45	7.99
25	0.41	0.98	1.54	2.11	2.67	3.24	3.81	4.37	4.94	5.51	6.07	6.64	7.20	7.77	8.34

Total NPV

[million CHF]

Mass flowrate (kg/s) \ Number of well	1.00	2.00	3.00	4.00	5.00	6.00	7.00	8.00	9.00	10.00	11.00	12.00	13.00	14.00	15.00
1.00	-64.73	-86.49	-108.25	-130.01	-151.77	-173.54	-195.30	-217.06	-238.82	-260.58	-282.34	-304.10	-325.86	-347.63	-369.39
2.00	-58.86	-73.94	-89.02	-104.10	-119.19	-134.27	-149.35	-164.43	-179.51	-194.60	-209.68	-224.76	-239.84	-254.93	-270.01
3.00	-52.98	-61.39	-69.79	-78.19	-86.60	-95.00	-103.40	-111.81	-120.21	-128.61	-137.02	-145.42	-153.82	-162.23	-170.63
4.00	-47.11	-48.84	-50.56	-52.28	-54.01	-55.73	-57.46	-59.18	-60.91	-62.63	-64.35	-66.08	-67.80	-69.53	-71.25
5.00	-41.24	-36.29	-31.33	-26.38	-21.42	-16.47	-11.51	-6.56	-1.60	3.35	8.31	13.26	18.22	23.17	28.13
6.00	-35.37	-23.73	-12.10	-0.47	11.17	22.80	34.44	46.07	57.70	69.34	80.97	92.61	104.24	115.87	127.51
7.00	-29.50	-11.18	7.13	25.44	43.76	62.07	80.38	98.70	117.01	135.32	153.63	171.95	190.26	208.57	226.89
8.00	-23.62	1.37	26.36	51.35	76.34	101.34	126.33	151.32	176.31	201.31	226.30	251.29	276.28	301.27	326.27
9.00	-17.75	13.92	45.59	77.26	108.93	140.60	172.28	203.95	235.62	267.29	298.96	330.63	362.30	393.97	425.64
10.00	-11.88	26.47	64.82	103.17	141.52	179.87	218.22	256.57	294.92	333.27	371.62	409.97	448.32	486.67	525.02
11.00	-6.01	39.02	84.05	129.08	174.11	219.14	264.17	309.20	354.23	399.26	444.29	489.31	534.34	579.37	624.40
12.00	-0.14	51.57	103.28	154.99	206.70	258.41	310.11	361.82	413.53	465.24	516.95	568.66	620.37	672.07	723.78
13.00	5.74	64.12	122.51	180.90	239.29	297.67	356.06	414.45	472.84	531.22	589.61	648.00	706.39	764.77	823.16
14.00	11.61	76.68	141.74	206.81	271.87	336.94	402.01	467.07	532.14	597.21	662.27	727.34	792.41	857.47	922.54
15.00	17.48	89.23	160.97	232.72	304.46	376.21	447.95	519.70	591.45	663.19	734.94	806.68	878.43	950.17	1'021.92
16.00	23.35	101.78	180.20	258.63	337.05	415.48	493.90	572.33	650.75	729.17	807.60	886.02	964.45	1'042.87	1'121.30
17.00	29.22	114.33	199.43	284.54	369.64	454.74	539.85	624.95	710.05	795.16	880.26	965.37	1'050.47	1'135.57	1'220.68
18.00	35.10	126.88	218.66	310.45	402.23	494.01	585.79	677.58	769.36	861.14	952.93	1'044.71	1'136.49	1'228.27	1'320.06
19.00	40.97	139.43	237.89	336.35	434.82	533.28	631.74	730.20	828.66	927.13	1'025.59	1'124.05	1'222.51	1'320.97	1'419.44
20.00	46.84	151.98	257.12	362.26	467.40	572.55	677.69	782.83	887.97	993.11	1'098.25	1'203.39	1'308.53	1'413.67	1'518.81
21.00	52.71	164.53	276.35	388.17	499.99	611.81	723.63	835.45	947.27	1'059.09	1'170.91	1'282.73	1'394.55	1'506.37	1'618.19
22.00	58.59	177.08	295.58	414.08	532.58	651.08	769.58	888.08	1'006.58	1'125.08	1'243.58	1'362.08	1'480.57	1'599.07	1'717.57
23.00	64.46	189.64	314.81	439.99	565.17	690.35	815.53	940.70	1'065.88	1'191.06	1'316.24	1'441.42	1'566.60	1'691.77	1'816.95
24.00	70.33	202.19	334.04	465.90	597.76	729.62	861.47	993.33	1'125.19	1'257.04	1'388.90	1'520.76	1'652.62	1'784.47	1'916.33
25.00	76.20	214.74	353.27	491.81	630.35	768.88	907.42	1'045.96	1'184.49	1'323.03	1'461.56	1'600.10	1'738.64	1'877.17	2'015.71

Figure 20: Sensitivity Analysis of Economic Viability for Different Configurations of Mass Flow Rate and Number of Wells showing valuable insights for optimizing system design and achieving economically feasible energy production configurations. This figure provides a comprehensive sensitivity analysis conducted using a "What-If scenarios to evaluate the influence of mass flow rate (kg/s) and the number of wells on key economic metrics. The analysis assumes the following fixed parameters: Thermal Energy Selling Price for direct heating at 0.15 CHF/kWh, and Grid Electricity Purchase Price at 0.01 CHF/kWh. (a) Payback Period: The payback period (in years) is assessed as a function of mass flow rate and the number of wells. The highlighted cells represent configurations achieving a payback period below economic thresholds, guiding the selection of efficient setups. The values marked as 999.00 indicate that the payback period cannot be achieved within the operational lifetime of the system under those specific conditions. (b) Net Annual Cash Flow: This subfigure illustrates the net annual cash flow (in million CHF/year) for varying combinations of mass flow rate and well count. Positive cash flows (green cells) indicate profitable setups, while negative cash flows (red cells) highlight economically unfeasible configurations. (c) Total Net Present Value (NPV): The NPV analysis (in million CHF) evaluates the long-term economic feasibility of configurations. Green cells represent scenarios with high profitability, while red cells denote setups failing to recover investment costs. A minimum mass flow rate of >13 kg/s with nine wells is identified as the baseline for economic viability.

We found that with one borehole, a massflow rate of >13 kg/s is the value to make this system run economically.

- **STEP 02: Selling thermal energy during winter vs buying electricity during summer to heat the fluid**

Building upon the first sensitivity analysis, where the optimal mass flow rate was determined to be 13 kg/s with 1 well, this analysis focuses on evaluating the economic trade-offs between selling thermal energy during winter and purchasing electricity during summer to heat the fluid. We assumed the following points:

- Thermal energy is sold during winter at rates ranging from 0.01 CHF/kWh to 0.25 CHF/kWh.
- Electricity purchase prices during summer vary between 0 CHF/kWh and 0.28 CHF/kWh. At 0 CHF/kWh for electricity, it is assumed that electricity is either sourced for free (e.g., from solar PV) or that the industrial complex provides the heated fluid at a temperature of 60°C, eliminating the need for electricity in the boiler.

Optimal Combination findings:

The analysis identifies that, for a mass flow rate of 13 kg/s with 1 well, a thermal energy selling price of at least 0.14 CHF/kWh combined with minimal electricity costs ensures profitability. As electricity costs increase, higher thermal energy selling prices are required to offset the expenses.

Payback Period

[years]

Thermal Energy Selling Price for district heating (CHF/kWh) \ Grid Electricity Price (CHF/kWh)	0	0.02	0.04	0.06	0.08	0.1	0.12	0.14	0.16	0.18	0.2	0.22	0.24	0.26	0.28
0.01	999.00	999.00	999.00	999.00	999.00	999.00	999.00	999.00	999.00	999.00	999.00	999.00	999.00	999.00	999.00
0.02	999.00	999.00	999.00	999.00	999.00	999.00	999.00	999.00	999.00	999.00	999.00	999.00	999.00	999.00	999.00
0.03	999.00	999.00	999.00	999.00	999.00	999.00	999.00	999.00	999.00	999.00	999.00	999.00	999.00	999.00	999.00
0.04	999.00	999.00	999.00	999.00	999.00	999.00	999.00	999.00	999.00	999.00	999.00	999.00	999.00	999.00	999.00
0.05	999.00	999.00	999.00	999.00	999.00	999.00	999.00	999.00	999.00	999.00	999.00	999.00	999.00	999.00	999.00
0.06	999.00	999.00	999.00	999.00	999.00	999.00	999.00	999.00	999.00	999.00	999.00	999.00	999.00	999.00	999.00
0.07	999.00	999.00	999.00	999.00	999.00	999.00	999.00	999.00	999.00	999.00	999.00	999.00	999.00	999.00	999.00
0.08	999.00	999.00	999.00	999.00	999.00	999.00	999.00	999.00	999.00	999.00	999.00	999.00	999.00	999.00	999.00
0.09	999.00	999.00	999.00	999.00	999.00	999.00	999.00	999.00	999.00	999.00	999.00	999.00	999.00	999.00	999.00
0.1	999.00	999.00	999.00	999.00	999.00	999.00	999.00	999.00	999.00	999.00	999.00	999.00	999.00	999.00	999.00
0.11	28.65	999.00	999.00	999.00	999.00	999.00	999.00	999.00	999.00	999.00	999.00	999.00	999.00	999.00	999.00
0.12	18.97	29.99	999.00	999.00	999.00	999.00	999.00	999.00	999.00	999.00	999.00	999.00	999.00	999.00	999.00
0.13	14.37	19.50	999.00	999.00	999.00	999.00	999.00	999.00	999.00	999.00	999.00	999.00	999.00	999.00	999.00
0.14	11.61	14.66	20.06	999.00	999.00	999.00	999.00	999.00	999.00	999.00	999.00	999.00	999.00	999.00	999.00
0.15	9.76	11.80	14.96	20.65	999.00	999.00	999.00	999.00	999.00	999.00	999.00	999.00	999.00	999.00	999.00
0.16	8.42	9.88	11.98	15.28	21.29	999.00	999.00	999.00	999.00	999.00	999.00	999.00	999.00	999.00	999.00
0.17	7.41	8.52	10.02	12.19	15.61	21.96	999.00	999.00	999.00	999.00	999.00	999.00	999.00	999.00	999.00
0.18	6.62	7.49	8.62	10.16	12.39	15.95	22.69	999.00	999.00	999.00	999.00	999.00	999.00	999.00	999.00
0.19	5.98	6.68	7.56	8.72	10.30	12.61	16.32	23.47	999.00	999.00	999.00	999.00	999.00	999.00	999.00
0.2	5.46	6.02	6.74	7.64	8.82	10.45	12.83	16.70	24.32	999.00	999.00	999.00	999.00	999.00	999.00
0.21	5.01	5.50	6.07	6.80	7.72	8.92	10.59	13.05	17.09	25.23	999.00	999.00	999.00	999.00	999.00
0.22	4.64	5.05	5.54	6.12	6.86	7.80	9.03	10.75	13.29	17.52	26.23	999.00	999.00	999.00	999.00
0.23	4.32	4.67	5.08	5.58	6.18	6.92	7.88	9.14	10.90	13.54	17.96	27.32	999.00	999.00	999.00
0.24	4.04	4.35	4.70	5.12	5.62	6.23	6.98	7.96	9.26	11.07	13.79	18.43	28.52	999.00	999.00
0.25	3.79	4.06	4.37	4.73	5.15	5.66	6.28	7.05	8.04	9.38	11.24	14.06	18.92	29.84	999.00

Net Annual Cash Flow

[million CHF/year]

Thermal Energy Selling Price for dirstect heating (CHF/kWh) \ Grid Electricity Price (CHF/kWh)	0	0.02	0.04	0.06	0.08	0.1	0.12	0.14	0.16	0.18	0.2	0.22	0.24	0.26	0.28
0.01	-0.12	-0.14	-0.16	-0.18	-0.20	-0.22	-0.25	-0.27	-0.29	-0.31	-0.33	-0.35	-0.37	-0.40	-0.42
0.02	-0.10	-0.12	-0.14	-0.16	-0.18	-0.21	-0.23	-0.25	-0.27	-0.29	-0.31	-0.33	-0.36	-0.38	-0.40
0.03	-0.08	-0.10	-0.12	-0.14	-0.16	-0.19	-0.21	-0.23	-0.25	-0.27	-0.29	-0.31	-0.34	-0.36	-0.38
0.04	-0.06	-0.08	-0.10	-0.12	-0.14	-0.17	-0.19	-0.21	-0.23	-0.25	-0.27	-0.29	-0.32	-0.34	-0.36
0.05	-0.04	-0.06	-0.08	-0.10	-0.12	-0.15	-0.17	-0.19	-0.21	-0.23	-0.25	-0.27	-0.30	-0.32	-0.34
0.06	-0.02	-0.04	-0.06	-0.08	-0.10	-0.13	-0.15	-0.17	-0.19	-0.21	-0.23	-0.25	-0.28	-0.30	-0.32
0.07	0.00	-0.02	-0.04	-0.06	-0.08	-0.11	-0.13	-0.15	-0.17	-0.19	-0.21	-0.23	-0.26	-0.28	-0.30
0.08	0.02	-0.00	-0.02	-0.04	-0.06	-0.09	-0.11	-0.13	-0.15	-0.17	-0.19	-0.21	-0.24	-0.26	-0.28
0.09	0.04	0.02	-0.00	-0.02	-0.05	-0.07	-0.09	-0.11	-0.13	-0.15	-0.17	-0.20	-0.22	-0.24	-0.26
0.1	0.06	0.04	0.02	-0.00	-0.03	-0.05	-0.07	-0.09	-0.11	-0.13	-0.15	-0.18	-0.20	-0.22	-0.24
0.11	0.08	0.06	0.04	0.02	-0.01	-0.03	-0.05	-0.07	-0.09	-0.11	-0.13	-0.16	-0.18	-0.20	-0.22
0.12	0.10	0.08	0.06	0.04	0.01	-0.01	-0.03	-0.05	-0.07	-0.09	-0.11	-0.14	-0.16	-0.18	-0.20
0.13	0.12	0.10	0.08	0.06	0.03	0.01	-0.01	-0.03	-0.05	-0.07	-0.09	-0.12	-0.14	-0.16	-0.18
0.14	0.14	0.12	0.10	0.08	0.05	0.03	0.01	-0.01	-0.03	-0.05	-0.07	-0.10	-0.12	-0.14	-0.16
0.15	0.16	0.14	0.12	0.09	0.07	0.05	0.03	0.01	-0.01	-0.03	-0.05	-0.08	-0.10	-0.12	-0.14
0.16	0.18	0.16	0.14	0.11	0.09	0.07	0.05	0.03	0.01	-0.01	-0.04	-0.06	-0.08	-0.10	-0.12
0.17	0.20	0.18	0.16	0.13	0.11	0.09	0.07	0.05	0.03	0.01	-0.02	-0.04	-0.06	-0.08	-0.10
0.18	0.22	0.20	0.18	0.15	0.13	0.11	0.09	0.07	0.05	0.03	0.00	-0.02	-0.04	-0.06	-0.08
0.19	0.24	0.22	0.20	0.17	0.15	0.13	0.11	0.09	0.07	0.05	0.02	0.00	-0.02	-0.04	-0.06
0.2	0.26	0.24	0.22	0.19	0.17	0.15	0.13	0.11	0.09	0.07	0.04	0.02	0.00	-0.02	-0.04
0.21	0.28	0.26	0.24	0.21	0.19	0.17	0.15	0.13	0.11	0.09	0.06	0.04	0.02	-0.00	-0.02
0.22	0.30	0.28	0.25	0.23	0.21	0.19	0.17	0.15	0.13	0.10	0.08	0.06	0.04	0.02	-0.00
0.23	0.32	0.30	0.27	0.25	0.23	0.21	0.19	0.17	0.15	0.12	0.10	0.08	0.06	0.04	0.02
0.24	0.34	0.32	0.29	0.27	0.25	0.23	0.21	0.19	0.17	0.14	0.12	0.10	0.08	0.06	0.04
0.25	0.36	0.34	0.31	0.29	0.27	0.25	0.23	0.21	0.19	0.16	0.14	0.12	0.10	0.08	0.06

Total NPV

[million CHF]

Thermal Energy Selling Price for dirstect heating (CHF/kWh) \ Grid Electricity Price (CHF/kWh)	0	0.02	0.04	0.06	0.08	0.1	0.12	0.14	0.16	0.18	0.2	0.22	0.24	0.26	0.28
0.01	-71.84	-78.10	-84.37	-90.63	-96.90	-103.17	-109.43	-115.70	-121.97	-128.23	-134.50	-140.77	-147.03	-153.30	-159.57
0.02	-66.05	-72.31	-78.58	-84.85	-91.11	-97.38	-103.65	-109.91	-116.18	-122.45	-128.71	-134.98	-141.25	-147.51	-153.78
0.03	-60.26	-66.52	-72.79	-79.06	-85.32	-91.59	-97.86	-104.12	-110.39	-116.66	-122.92	-129.19	-135.46	-141.72	-147.99
0.04	-54.47	-60.74	-67.00	-73.27	-79.54	-85.80	-92.07	-98.34	-104.60	-110.87	-117.14	-123.40	-129.67	-135.94	-142.20
0.05	-48.68	-54.95	-61.21	-67.48	-73.75	-80.01	-86.28	-92.55	-98.81	-105.08	-111.35	-117.61	-123.88	-130.15	-136.41
0.06	-42.89	-49.16	-55.43	-61.69	-67.96	-74.23	-80.49	-86.76	-93.03	-99.29	-105.56	-111.83	-118.09	-124.36	-130.62
0.07	-37.10	-43.37	-49.64	-55.90	-62.17	-68.44	-74.70	-80.97	-87.24	-93.50	-99.77	-106.04	-112.30	-118.57	-124.84
0.08	-31.32	-37.58	-43.85	-50.12	-56.38	-62.65	-68.92	-75.18	-81.45	-87.71	-93.98	-100.25	-106.51	-112.78	-119.05
0.09	-25.53	-31.79	-38.06	-44.33	-50.59	-56.86	-63.13	-69.39	-75.66	-81.93	-88.19	-94.46	-100.73	-106.99	-113.26
0.1	-19.74	-26.01	-32.27	-38.54	-44.80	-51.07	-57.34	-63.60	-69.87	-76.14	-82.40	-88.67	-94.94	-101.20	-107.47
0.11	-13.95	-20.22	-26.48	-32.75	-39.02	-45.28	-51.55	-57.82	-64.08	-70.35	-76.62	-82.88	-89.15	-95.42	-101.68
0.12	-8.16	-14.43	-20.69	-26.96	-33.23	-39.49	-45.76	-52.03	-58.29	-64.56	-70.83	-77.09	-83.36	-89.63	-95.89
0.13	-2.37	-8.64	-14.91	-21.17	-27.44	-33.71	-39.97	-46.24	-52.51	-58.77	-65.04	-71.31	-77.57	-83.84	-90.11
0.14	3.42	-2.85	-9.12	-15.38	-21.65	-27.92	-34.18	-40.45	-46.72	-52.98	-59.25	-65.52	-71.78	-78.05	-84.32
0.15	9.20	2.94	-3.33	-9.60	-15.86	-22.13	-28.40	-34.66	-40.93	-47.20	-53.46	-59.73	-65.99	-72.26	-78.53
0.16	14.99	8.73	2.46	-3.81	-10.07	-16.34	-22.61	-28.87	-35.14	-41.41	-47.67	-53.94	-60.21	-66.47	-72.74
0.17	20.78	14.51	8.25	1.98	-4.29	-10.55	-16.82	-23.08	-29.35	-35.62	-41.88	-48.15	-54.42	-60.68	-66.95
0.18	26.57	20.30	14.04	7.77	1.50	-4.76	-11.03	-17.30	-23.56	-29.83	-36.10	-42.36	-48.63	-54.90	-61.16
0.19	32.36	26.09	19.83	13.56	7.29	1.03	-5.24	-11.51	-17.77	-24.04	-30.31	-36.57	-42.84	-49.11	-55.37
0.2	38.15	31.88	25.61	19.35	13.08	6.81	0.55	-5.72	-11.99	-18.25	-24.52	-30.79	-37.05	-43.32	-49.59
0.21	43.94	37.67	31.40	25.14	18.87	12.60	6.34	0.07	-6.20	-12.46	-18.73	-25.00	-31.26	-37.53	-43.80
0.22	49.72	43.46	37.19	30.92	24.66	18.39	12.12	5.86	-0.41	-6.68	-12.94	-19.21	-25.48	-31.74	-38.01
0.23	55.51	49.25	42.98	36.71	30.45	24.18	17.91	11.65	5.38	-0.89	-7.15	-13.42	-19.69	-25.95	-32.22
0.24	61.30	55.03	48.77	42.50	36.23	29.97	23.70	17.43	11.17	4.90	-1.36	-7.63	-13.90	-20.16	-26.43
0.25	67.09	60.82	54.56	48.29	42.02	35.76	29.49	23.22	16.96	10.69	4.42	-1.84	-8.11	-14.38	-20.64

In conclusion, we provide an initial economic assessment based on standard industry practices and available data. Further refinements can be made with additional financial inputs and market-specific considerations. The analysis is based on available data and reasonable industry assumptions. Any variations in actual values may affect the final financial outcomes. It is recommended to validate these assumptions with real-world project specifications before final decision-making.

Eventually, the thermal-hydraulic and the economic models will be validated against the basic operational parameters, e.g. flow volume, temperature, cycle properties. These parameters obtained during the experiments define the efficiency of the system, which can be compared to the numerically predicted efficiencies.

Sensitivity to reservoir temperature

In Figure 21, we compare different configurations of injection and reservoir temperature. Even a low reservoir temperature of 25°C, economic heat storage is viable, for instance at high injection temperature. The economics degrade with lower injection temperature and reservoir temperature.

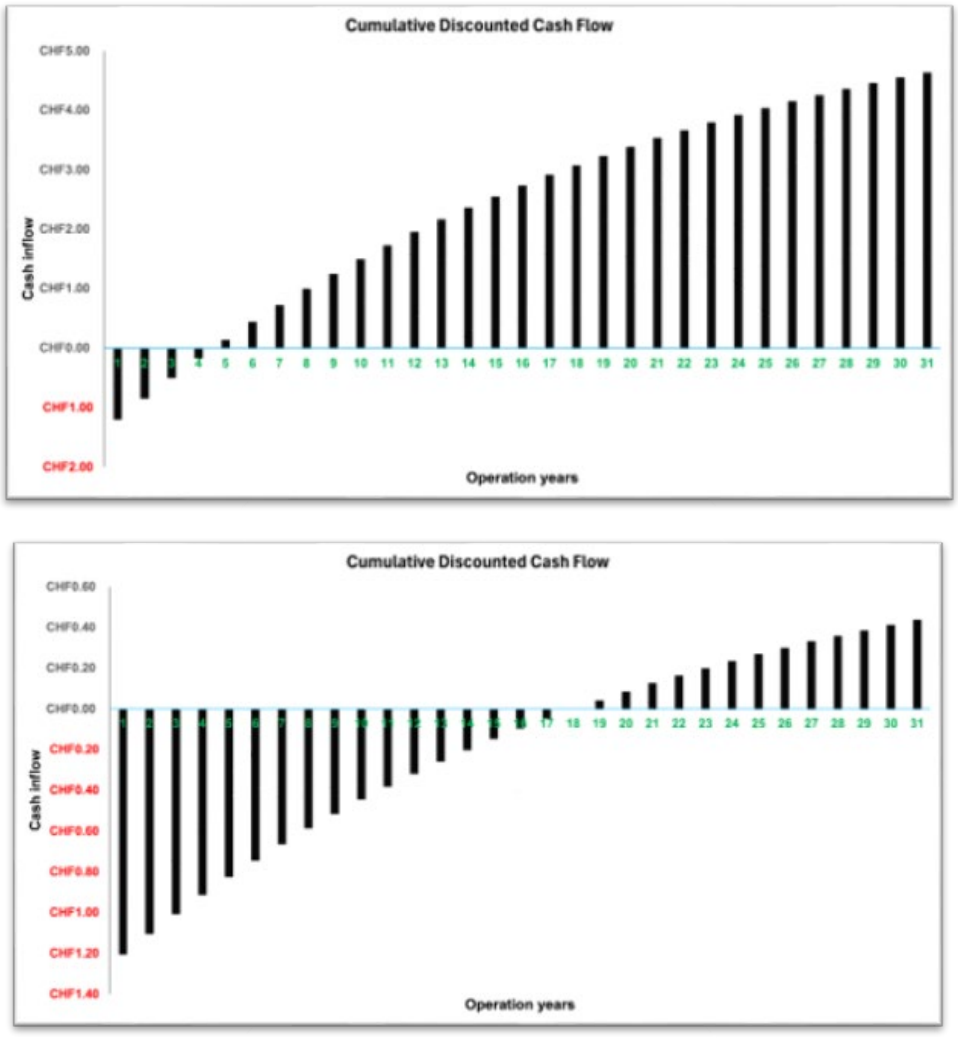

Figure 21: Sensitivity of cash flow model to different injection and reservoir temperatures. Top: Injection temperature: 80 ℃, Reservoir Temperature at 500 meters: 25 ℃, Production Temperature: 60 ℃, Bottom: Injection Temperature: 40 ℃, Reservoir Temperature at 500 meters: 15 ℃ Production Temperature: 30 ℃

2.5 Preliminary conceptual design of the first experiment

The purpose of the first experiment in the BedrettoLab is to proof the technical feasibility of injecting/extracting heat in a fractured granite. In this section, we describe in detail the set-up necessary for the execution of the first heating experiment in the BedrettoLab., which includes (1) the selection of the borehole and the injection interval (Sections 2.5.1 and 2.5.2, respectively), the forecast using the base model described in Section 2.1 (Section 2.5.3), and the technical equipment (Section 2.5.4).

2.5.1. Proposed load/unload schedule

The model described in Section 2.1 was calibrated using available data at interval 11 (*Figure 22*). Overall, the major trends of measured pressures are properly captured. At early times of stimulation, the model underestimates pressure build-up during the first injection and recovery, i.e., it slightly overestimates transmissivity. This is attributed to either (1) a small overestimation of the evolving size of the stimulated fracture implemented in the model, or (2) a small mismatch in the modelling of the temperature of the injected fluid. Available data of the final 3-day long hydrotest are properly captured, which reveals that the calibrated transmissivity properly represents the transmissivity of the system. The mismatch to measured pressures during the final recovery may be attributed to many different factors, including system's compliance that are difficult, even hardly possible, to evaluate with a numerical model.

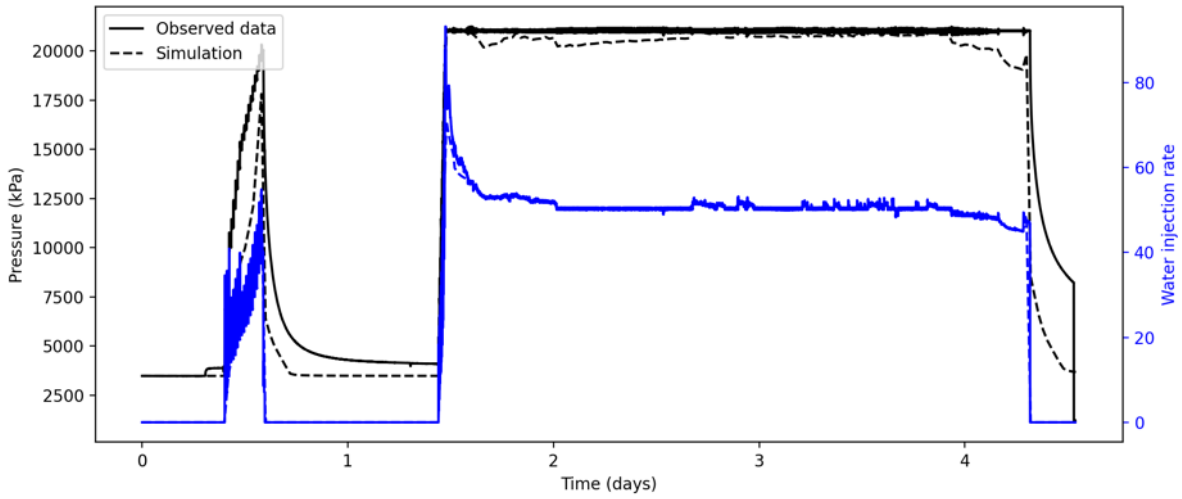

Figure 22 Calculated vs measured pressures at interval 11 using the numerical model.

The calibrated model was used to simulate realistic injection schemes and to design the set-up of the first heat injection experiment. To keep seismicity under tolerable levels, it is decided to keep downhole pressure at 15 MPa, slightly above the jacking pressure necessary to enhance the small initial aperture. According to these boundary conditions, we decided to execute a 1-month load-and-unload cycle only, without resting cycle between load and unload with the primary goal to demonstrate the feasibility of heat injection/extraction only and not with the intent to maximize efficiency

During load, the inflow is kept at the wellhead at a temperature of 60°. Energy extraction is achieved by opening the hole, i.e., under natural back-flow conditions, although the possibility of setting a small pump downhole to increase the production rate is being evaluated. Two load-unload schemes, in the presence

and absence of resting period between load and unload, have been tested (Figure 23). In both cases, the retrieved volume of water is 20-30%, which approximately corresponds to the measured back-flow during the previous stimulations. The scheme without resting cycles is finally chosen because (1) retrieved volumes are larger (because indeed injected volumes are larger too), and (2) the temperature level is more constant during the unload cycle.

Figure 23 Calculated temperatures and flow rates in response to two different load-unload cycles. On top, hot water is loaded for one week. This cycle is followed by a 1-week resting period, a 1-week unload cycle under open-hole conditions, and a final closure of the well for 1 week. On bottom, resting cycles are removed.

A rough look to the latest available data set in interval 11 (Figure 24) reveals that, under 15 MPa downhole pressure, the inflow was ca. 10 L/min during the HTPF test at day1 and ca. 15 L/min during the controlled flow rate test (day 2). Under the aforementioned downhole pressure conditions, the model estimates an inflow 2.5 times larger (about 52 m3/d or 36 L/min). This is an effect of the cold temperature of the injected fluid during stimulation. None the less, it is expected (in view of previous stimulation campaign) that slightly rising the downhole pressure will lead to higher inflows and outflows, thus improving efficiency.

In addition, injecting hot fluid decreases fluid density (which tends to lower hydraulic conductivity, and therefore transmissivity) and dynamic viscosity (which tends to increase transmissivity, and correspondingly inflows and outflows):

$$K = \frac{\rho g \kappa}{\mu}$$

where K[m/s] is hydraulic conductivity, ρ [kg/m3] is fluid density, g is gravity [m/s2], κ [m2] is intrinsic permeability, and μ [Kg/m/s)] is fluid viscosity. Two phenomena compete as temperature increases. On

the one hand, fluid density diminishes. However, the dominant effect is the decrease of fluid viscosity. For the suggested experiment, i.e., injecting hot fluid, it is expected that transmissivity will increase a factor 2.1 - 2.8 with respect to the natural baseline value after stimulation. Equivalently, inflow will increase to 30-45 L/min, which is precisely the amount predicted by the model. The adjustment of downhole pressure and temperature will be carried out in the field if it is observed that induced seismicity does not pose any additional risk.

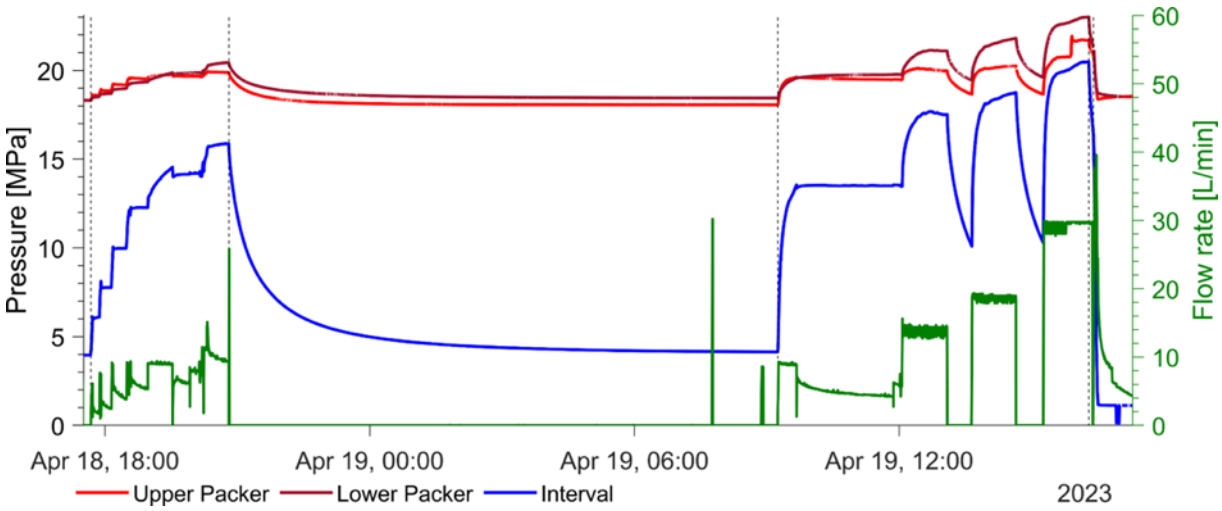

Figure 24 Measured downhole pressures and corresponding inflows after the VALTER Phase 2 stimulation of interval 11.

To better ascertain the parameterization (especially the initial transmissivity), a prior hydrotest will be carried out in Interval 11, whose interpretation will yield the actual initial conditions for the injection experiment.

To enhance efficiency of the system, it is proposed to empty first the annulus above Internal 14 because heat losses diminish due to the presence of air surrounding the piping. This possibility has not yet been included in the model. In the same line of arguments, all flow lines will be insulated from the heater to the wellhead. During the whole duration of the experiment, temperatures and pressures at all intervals of ST1 and at monitoring boreholes nearby will be measured. In addition, the HQ (high-quality) seismic surveillance will be monitoring all operations.

The collected data sets will be implemented in the existing model and parameter calibration will be carried out to reproduce measured flow rates and temperatures. The model will then be utilized for simulating more realistic injection schemes for posterior phases of the BEACH project including, e.g., a dipole scheme involving borehole ST2.

2.5.2. Technical equipment and surface-surface flow lines

The heating power during the load cycle the has been estimated by considering a maximum inflow of 60 m^3/d (42 L/min) and a maximum differential temperature of 40°C (temperature at wellhead of 60°C and temperature in the formation ca. 20°C. This leads to a maximum nominal power of 220 kW. The electrically powered industrial heater to be utilized is designed for continuous operation, offering a consistent flow rate between 10 and 40 L/min over durations ranging from one to two weeks. It is engineered to manage an inflow temperature of approximately 15°C (that of the water from the lateral drainage channel), raising the fluid temperature to between 60°C and 90°C at the outlet of the heater and the

wellhead. With compact dimensions of approximately 2x1.5x2 meters (notably, it can be tilted), the heater will fit seamlessly within the gallery and can be easily transported to the TM2000 unit next to the injection well, minimizing the need for extensive and inefficient piping, e.g. to wider sections of the tunnel or, worst, to the exterior. The heater is compatible with inlet pumps and can handle inlet pressures between 4 and 10 bar. The outlet is designed to interface with high pressure pumps, allowing further pressurization of the fluid. The power supply utilizes standard EN60309 industrial plugs, fully compatible with the lab's electrical grid, and will feature its own internal circuit breakers for added security. Figure 25 sketches the hydraulic and data lines. Notably, most of the equipment is already present at Bedretto. In addition, it has been checked with service companies delivering heaters to ascertain the cost of renting the heater, its size and the delivery times.

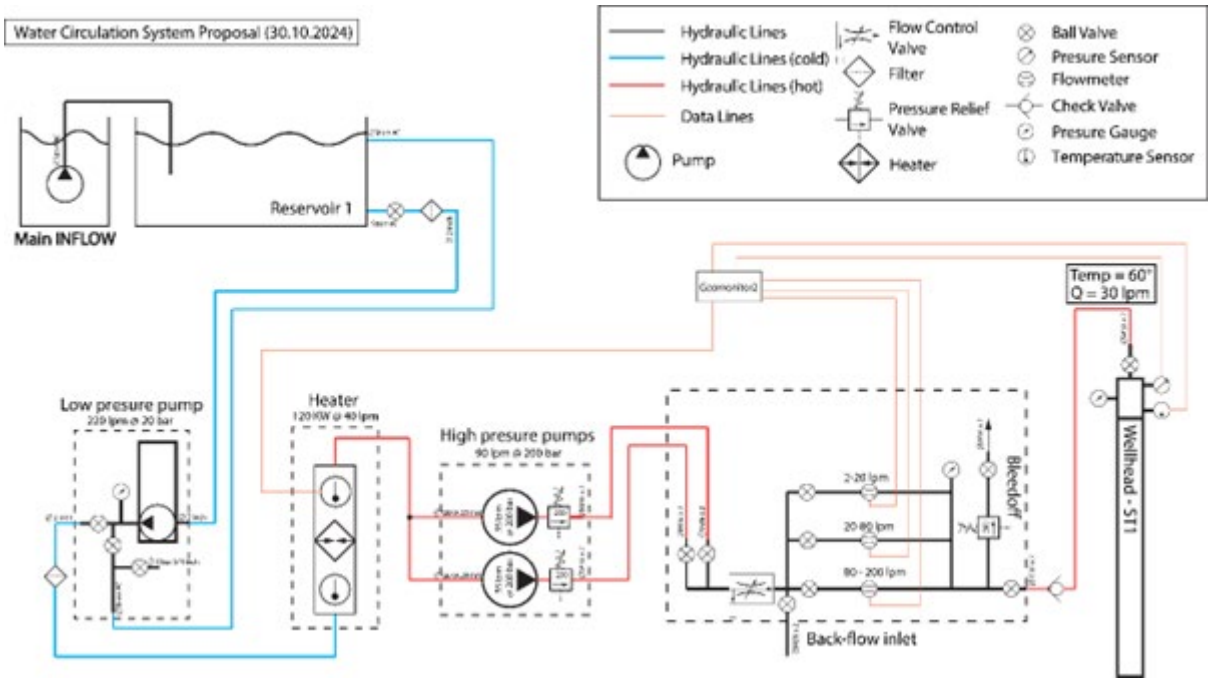

Figure 25 Preliminary design of hydraulic and data lines.

3 Conclusions and outlook

The first Phase of the BEACH project concludes with a good theoretical understanding of the behaviour of fractured rocks during heat storage. Using numerical reservoir simulations and techno-economic analysis we investigated potential locations for FTES in Switzerland. The locations are at different development stages from reconnaissance studies to theoretically operating fields. This wide range allows to analyze different aspects of FTES systems.

Studying fracture systems at surface in advance to project development turns out to be crucial. Fracture spacing, shape factor and anisotropy define the fracture networks. Its study in outcrops close to the project development phase reveals information if the fractures penetrate throughout the rock into the potential reservoir and their connectivity for potential transport of fluids. Additionally, it is important to analyse surface facilities. We mapped heat emitting sites, e.g. waste incineration plants, against potential reservoir rocks. A potential site for a future FTES project is at Uvrier, where a waste incineration plant is producing excess heat. This location is close to the hot springs at Leukerbad, which indicates a conductive fractured rock system transporting warm water. A more detailed study at the Schaffhausen site indicates good properties of crystalline rock for FTES with an efficiency exceeding 100%, at certain depths. For the site X (undisclosed for confidentiality) we conducted a tecno-economic analysis and found a payback period of 9 years for an FTES system at that location.

The most detailed numerical study was conducted at the BedrettoLab site, an underground laboratory for testing geoscientific and geo-energy technologies. We modelled several FTES cycles to test the feasibility and efficiency of storing heat in the Bedretto reservoir. We were able to prove the technical feasibility with an efficiency of >70%. A detailed technical design study was conducted to plan the next phase of BEACH. We decided to use interval 11 of the ST1 borehole to conduct the first experiments, planned for early 2025.

We conclude that FTES is a feasible technology for the Swiss energy market. It makes use of the fractured rocks covering most of the underground of Switzerland. It can buffer energy excess by storing heat and making it available in times when its needed. Various sites in the country are feasible to install such systems, where surface facilities are available and the underground has suitable properties. The Bedretto test site is ready for conducting the first experiments to prove the consistency between models and experiments.

National and international cooperation

Industry collaboration with AET

A close collaboration is held with the industry partner AET. AET directors and engineers visited the BedrettoLab on 12 June 2024 together with the ETH Team to get an overview of the tunnel infrastructure and available equipment in the laboratory. The team walked along the whole tunnel length, investigated geologically interesting sites and discussed possible experiment setups in the laboratory with the current borehole installations and instrumentation.

Figure 26 Visit of AET to the BedrettoLab

Support of the Canton Ticino

On July 18th, 2024, we met with members of the Administration of the Department of the Territory of the Canton Ticino to present the objectives of the BEACH project. The Canton expressed strong support for the project and emphasized the importance of integrating energy storage solutions into its current energy strategy. Specifically, the Canton Ticino has committed to supporting the project in the following ways:

- **Incorporating the BEACH project into the PECC (Cantonal Energy and Climate Strategy)** as a pilot initiative. The PECC is currently under review by the Cantonal parliament and is expected to be voted on soon (refer to page 200 of the document: https://www4.ti.ch/fileadmin/GENERALE/PECC/documenti/PECC2024_24.10.24.pdf).
- **Including heat accumulator systems in the FER funding program** (https://www4.ti.ch/generale/fer/home), thereby increasing BEACH's eligibility for financial support under this scheme.
- **Providing overall project support**, with further actions to be discussed and defined as the project progresses to subsequent stages.

Collaboration with an industrial partner in northern Switzerland

A collaboration has been started with preparing Letters of interest in October 2024. The collaboration is with an industry park including EWZ, a biomass power plant, a woodfire power plant and EPSF.

4 Publications and other communications

1. The BEACH consortium already published on the topic of using and storing heat in the Bedretto tunnel. One of the articles is online and featured on the frontpage of the journal and one other in under review currently. Link to 1. publication: https://www.mdpi.com/1996-1073/17/15
2. Regarding dissemination and outreach we had 2 main activities:
    a. On Saturday, September 7, 2024, we presented the BEACH project to the public at the Piazza del Sole in Bellinzona, as part of the Greenday Festival. The Greenday Festival focused on promoting sustainability and nature conservation through engaging, fun-filled activities. The festival offered a variety of experiences, including music, entertainment, interactive workshops, nature trails, games, and quizzes, all designed to inspire a more sustainable lifestyle. Our booth for the BEACH project attracted a diverse and steady stream of visitors, with many families and children showing interest throughout the day. The project's focus on energy storage in fractured rock was met with interest and curiosity, and we got overall positive feedback from the audience.
    b. An SRF reportage was filmed about the BEACH project idea and broadcasted in ‚10 vor 10 - Die Idee': https://www.srf.ch/play/tv/10-vor-10/video/die-idee-waermespeicherung-im-gestein?urn=urn:srf:video:a17468c8-1525-4717-9095-a184fd5bf622

5 References

Bhark, Eric, and Kaveh Dehghani. "Assisted history matching benchmarking: Design of experiments-based techniques." In *SPE Annual Technical Conference and Exhibition*, pp. SPE-170690. SPE, 2014.

Bröker K., Ma X., Gholizadeh N. et al. (2024). Hydromechanical characterization of a fractured crystalline rock volume during multi-stage hydraulic stimulations at the BedrettoLab. Geothermics 124 (2024) 103126.

Bröker, K., Ma, X., Zhang, S., Gholizadeh N. et al. (2024). Constraining the stress field and its variability at the BedrettoLab: Elaborated hydraulic fracture trace analysis. Int. J. Rock Mech. Min. Sci. 178, 105739. http://dx.doi.org/10.1016/j.ijrmms.2024. 105739.

Castilla, R., Krietsch, H., Jordan et al. (2021). Conceptual geological model of the bedretto underground laboratory for geoenergies. In: 82nd EAGE Annual Conference & Exhibition, Vol. 2021. European Association of Geoscientists & Engineers, http://dx.doi.org/10.3997/2214-4609.202011912.

de La Bernardie, J., Bour, O., Le Borgne, T., Guihéneuf, N., Chatton, E., Labasque, T., ... & Gerard, M. F. (2018). Thermal attenuation and lag time in fractured rock: Theory and field measurements from joint heat and solute tracer tests. *Water Resources Research*, *54*(12), 10-053.

Gholizadeh Doonechaly N., Bröker K., Ma X., Scarabello L., Villiger L., Wenning Q., Rinaldi A. P., Repollés V. C., Shakas A., Hertrich M., Obermann A., ,, Plenkers K., Maurer H., Wiemer S., Giardini D. and Team B. (2023). "Flow Path Alterations during Hydraulic Stimulation at Bedretto Underground Laboratory for Geosciences and Geoenergies." Geothermal Resources Council Transactions 47: 2746-2759.

Gholizadeh Doonechaly N., Bröker K., Hertrich M., Rosskopf M., Obermann A., Durand V., Serbeto F., Shakas A., Ma X., Rinaldi A. P., Clasen Repollés V., Villiger L., Meier M., Gischig V., Plenkers K., Maurer H., Wiemer S. and Giardini D. (2024). "Insights from Subsurface Monitoring for Engineering of the Stimulation Pattern in Fractured Reservoirs." Rock Mechanics and Rock Engineering Submitted DOI: Preprint available at: https://doi.org/10.21203/rs.3.rs-4859925/v1.

Giardini, Domenico, Wiemer, Stefan, Maurer, Hansruedi, Hertrich, Marian, Meier, Peter, Alcolea, Andres, Castilla, Raymi, Hochreutener, Rebecca, 2022, Validation of Technologies for reservoir engineering (VALTER), Swiss Federal Office of Energy SFOE

Helton, Jon C., and Freddie Joe Davis. "Latin hypercube sampling and the propagation of uncertainty in analyses of complex systems." *Reliability Engineering & System Safety* 81, no. 1 (2003): 23-69.

Hertrich, M., Brixel, B., Bröker, K., et al. (2021). Characterization, hydraulic stimulation, and fluid circulation experiments in the bedretto underground laboratory for geosciences and geoenergies. In: 55th U.S. Rock Mechanics/Geomechanics Symposium. Virtual, June 2021.

Huenges, Ernst, Ellis, Justyna, Marti, Michele, Valenzuela, Nadja, 2020, Demonstration of soft stimulation treatments of geothermal reservoirs (DESTRESS), European Commission

Klepikova, M., Méheust, Y., Roques, C., & Linde, N. (2021). Heat transport by flow through rough rock fractures: a numerical investigation. *Advances in Water Resources*, *156*, 104042.

Knobloch, K., Ulrich, T., Bahl, C., & Engelbrecht, K. (2022). Degradation of a rock bed thermal energy storage system. *Applied Thermal Engineering*, *214*, 118823.

Lützenkirchen, V., Löw, S., 2011. Late Alpine brittle faulting in the Rotondo granite (Switzerland): deformation mechanisms and fault evolution. Swiss J. Geosci. 104 (1), 31–54. http://dx.doi.org/10.1007/s00015-010-0050-0.

Ma, X., Hertrich, M., Amann, F., et al. (2022). Multi-disciplinary characterizations of the BedrettoLab – a new underground geoscience research facility. Solid Earth 13 (2), 301–322. http://dx.doi.org/10.5194/se-13-301-2022.

Meier, Peter, Christe, Fabien, 2023, Zonal Isolation, Drilling and Exploitation of EGS Projects (Zodrex), Swiss Federal Office of Energy SFOE

Merkofer, R., Brehme, M., Shor, RJ. (2024) Evaluation of the geothermal energy potential of Switzerland- a techno-economic approach, PROCEEDINGS, 49th Workshop on Geothermal Reservoir Engineering Stanford University, Stanford, California, February 12-14, 2024 SGP-TR-227

Obermann A., Rosskopf M., Durand V., Plenkers K., Bröker K., Rinaldi A. P., Gholizadeh Doonechaly N., Gischig V., Zappone A., Amann F., Cocco M., Hertrich M., Jalali M., Junker J. S., Kästli P., Ma X., Maurer H., Meier M.-A., Schwarz M., Selvadurai P., Villiger L., Wiemer S., Dal Zilio L. and Giardini D. (2024). "Seismic Response of Hectometer-Scale Fracture Systems to Hydraulic Stimulation in the Bedretto Underground Laboratory, Switzerland." Journal of Geophysical Research: Solid Earth 129(11): e2024JB029836 DOI: https://doi.org/10.1029/2024JB029836.

Pozzoni, M. and Schenker, F. L. and Spataro, A. and Corboud, F. (2018) Estrazione pietra naturale nel comparto di Riveo-Visletto (Vallemaggia) - Studio della situazione attuale e possibili scenari di sviluppo della cave di pietra di Riveo-Visletto. Project Report. http://repository.supsi.ch/id/eprint/11322

Rast, M., Galli, A., Ruh, J.B et al. (2022). Geology along the Bedretto tunnel: kinematic and geochronological constraints on the evolution of the Gotthard Massif (Central Alps). Swiss J. Geosci. 115, 8. http://dx.doi.org/10. 1186/s00015-022-00409-w.

SRF, 8.11.2024, https://www.srf.ch/news/schweiz/umstrittene-forderung-solaranlagen-sollen-gedrosselt-werden-koennen

Wenning, Q. C., Gholizadeh Doonechaly, N., Shakas, A., Hertrich, M., Maurer, H., Giardini, D., ... & Wiemer, S. (2022, June). Heat propagation through fractures during hydraulic stimulation in crystalline rock. In *ARMA US Rock Mechanics/Geomechanics Symposium* (pp. ARMA-2022). ARMA.

Zhou, R., Zhan, H., & Wang, Y. (2022). On the role of rock matrix to heat transfer in a fracture-rock matrix system. *Journal of contaminant hydrology*, *245*, 103950.

6 Appendix

6.1 CFD model development

In parallel to the aforementioned modeling approach, an alternative modeling strategy is also under exploration. As opposed to the former, the difference of this alternative modeling approach is the exploitation of computational fluid dynamics (CFD), based on finite volume method (FVM), to solve the governing equations of mass, momentum and energy.
With this alternative modeling approach, detailed fluid-solid interaction analysis at small scale can be effectively performed; besides that, an agile model suitable to replicate the thermo-fluid dynamics behavior, and to assess the transient performance, of a generic large scale FTES system will also be developed. This work is in progress, more details can be found in the appendix.
Thanks to the large amount of information available, the BedrettoLab facility was assumed as reference for the numerical model development and validation. The latter aims at describing fluid flow inside the reservoir during injection/production processes through ST1 borehole, as well as assessing heat transfer phenomena in the fractured rock.
As the topological characteristics of the rock formations include a large number of fractures with a very reduced aperture (with respect to the reservoir scale), it is unfeasible to produce a computational grid integrating the actual geometrical representation of every single fracture. This is mainly due to difficulties in generating a numerical grid able to accurately capture the physical phenomena entailed in such a system: the typical length scale of a fracture (aperture wise) is in the order of millimeters, while reservoir scale can reach up to kilometers; this considerable difference restricts the meshing capabilities both from a grid size perspective (enormous computational effort) and from a cell quality standpoint (very challenging to obtain properly sized cells with sufficient quality).
For a more agile CFD model, porous media approach should be exploited. The major advantage of the latter is that no complete topological representation of the fractured media is required since the porous reservoir is modelled as a multiphase volume containing a solid matrix and interconnected voids (given porosity). An additional momentum source term (sink) is added to the standard governing momentum equations, composed of two parts: a viscous loss term and an inertial loss term. The latter parameters, in the momentum sink term, are permeability and inertial resistance coefficient, and can be defined through correlations already available and validated from the literature.
Heat transfer between the solid and the fluid phases can be replicated exploiting the so-called local thermal equilibrium (LTE) approach (i.e., fluid and solid temperatures are assumed to be locally equal), or by imposing a finite heat transfer coefficient that relates to conjugate heat transfer between the two phases (Local Thermal Non-Equilibrium, LTNE). Concerning the latter, the heat transfer coefficient must be properly assessed to reliably replicate heat transfer; correlations, already available in the literature, can be exploited to estimate its value. Furthermore, if needed, a variable heat transfer coefficient can also be considered.
As first attempt, an ideal reservoir was modelled by means of a 2D-axialsymmetric domain, where the symmetry axis lies on the centerline of the injection/production borehole (see Figure 27).

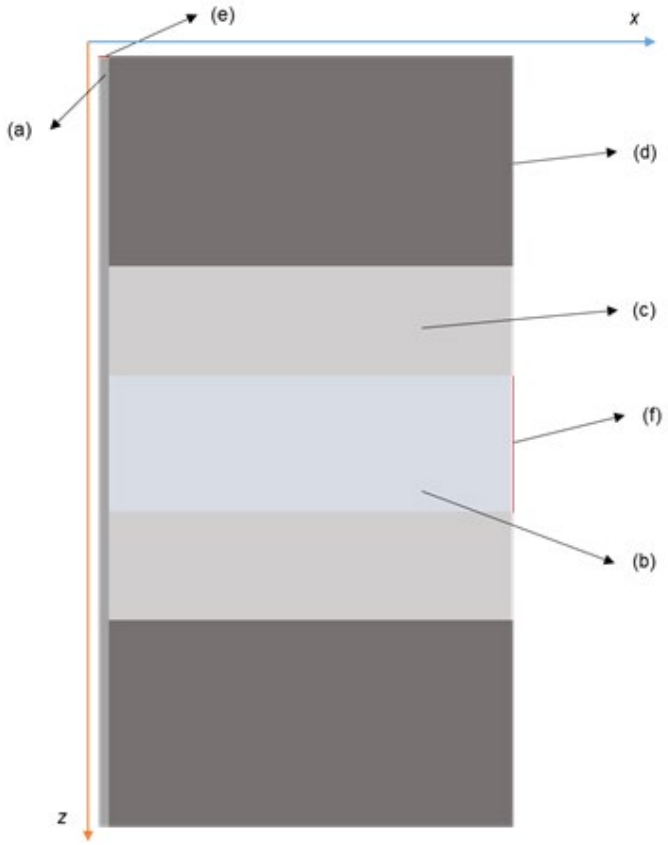

Figure 27 2D axis-symmetric model of the FTES approximated domain. (a), (b), (c) and (d) indicates the location in the computational domain characterized by different permeability values; (e) represents the heat transfer fluid inlet/outlet section during charging/discharging and (f) is the heat transfer fluid outlet/inlet section during discharging/charging.

The axis-symmetric fractured rock domain, represented in Figure 27, is subdivided in three different categories based on their expected permeability:

- (a) Fluid Borehole: this section of the domain represents the injection/production borehole, extending throughout the entire domain height (*z-axis coordinate*).
- (b) Fracture zone: porous media approach is applied to this cell zone with a given porosity value properly set. This zone is characterized by a higher permeability in the direction parallel to the fracture plane to account for anisotropy effects. Inertial coefficients are neglected.
- (c) Transition zone: a semi-permeable zone with isotropic permeability (lower than fracture zone permeabilities) to account for a possible “buffer” layer between the fracture zone and the solid crystalline rock zone. Inertial coefficients are neglected in this case also.
- (d) Solid crystalline rock: an impermeable zone representing the rock volumes surrounding the approximated fracture zone.

In Figure 27, the inlet and outlet section for the injection phase are designated with indexes (e) and (f) respectively; for the production phase, these boundary conditions are swapped, as (f) becomes the fluid inlet section and (e) turns accordingly into a pressure-outlet.

However, if a FTES with peripheral boreholes needs to be modelled, a limitation of this approach lies in the definition of the farthest lateral section of the fracture zone from the borehole centreline as outlet/inlet for the injection and production phases respectively ((f) in Figure 27). In fact, due to axial-symmetry, the latter section will be revolved around the borehole centreline, generating a very large surface area in which water is collected/injected. As this area is generated from the revolution of the entire lateral side of the fracture zone, it will not be representative of an actual production borehole, which would have a much smaller cross section. This limitation would inevitably affect the process efficiency and water recovery yield, as the operating fluid would be injected/collected from a much larger surface area, increasing thermal efficiency.
As the latter limitation suggests, a 2D axial symmetric domain should not be employed if the reservoir needs to be modelled with peripheral boreholes. Additionally, the latter model would not be suitable for the representation of the Bedretto Fractured Reservoir as the fracture zone would only take into account a small number of fractures parallel between each other (according to the anisotropic definition of permeability in this zone); as schematically depicted in Figure 27, this would not be the case of the Bedretto research area, where fractures are located with a much more stochastic distribution, with non-negligible interconnectivity between them, and also extending in a much larger “height” of the reservoir. Considering these limitations, the necessity for a more appropriate CFD model arises: this model should include at least an approximated topological definition of the fracture network shown in Figure 27 to properly represent fluid flow in a fractured media.

In this effort, the model domain was developed as a single porosity block with manually implemented viscous resistance profiles through User Defined Functions (UDFs), i.e., a “C” routine properly written to be integrated in the CFD solver, using the commercial software Fluent from ANSYS.
As aforementioned, the viscous resistance profile in a porous medium is governed by a sink term in the momentum transport equation; the parameters regarding viscous and inertial losses are inverse absolute permeability and inertial coefficient respectively.
The scope of this modelling approach is to maintain the porous media approximation integrating variable permeability and inertial coefficients based on spatial location inside the reservoir. To do that, the spatial distribution of the fractures needs to be identified.
Cartesian point clouds, representing each fracture in the Discrete Fracture Network (DFN) mapped for the Bedretto facility (see Figure 27), are derived and each fracture is then approximated as a surface plane built on a regression of the latter point cloud (Least square fitting of a plane onto a 3-dimensional point cloud).
These planes are referred to as “Fracture planes” in the UDF, and fracture aperture is defined as a constant “thickness” parameter: the latter plane functions are implemented in the UDF as z(x,y) cartesian functions (see Figure 28).

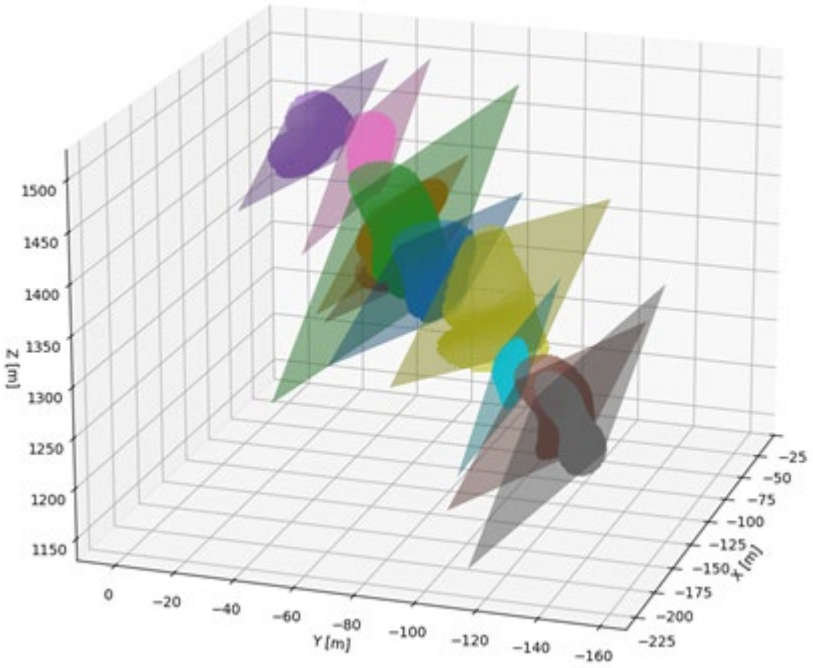

Figure 28 DFN domain where each fracture is represented by its point cloud and its relative plane fitting.

To every cell that lies in the cartesian coordinates range, defined by the fracture plane, is given a higher permeability with respect to the cells outside the fracture planes (3 to 4 orders of magnitude higher): higher permeability values are applied to these surfaces to account for preferential flow paths, symbolising the fractures, and lower permeabilities are applied to the rest of the domain to represent the solid crystalline rocks. By exploiting this UDF, fluid flow inside the single porosity block is governed by anisotropic viscous resistance profiles, thereby representing an eventual water flow through a fractured reservoir.
Inertial coefficients can also be applied to these points, as well as the parameters for an eventual LTNE model (e.g.: Interfacial area density, Heat transfer coefficient).

The expected results of this alternative model will mainly be: transient fluid and solid temperature distribution within the computational domain, evolution of the pressure and flow field during charging and discharging, quantification of the transient efficiency of the system.

6.2 Temperature Database

In the Northern part of Switzerland, extensive investigations have been conducted by Nagra (Swiss 10 National Cooperative for the Disposal of Radioactive Waste) to explore thesubsurface in relation to finding the most suitable site for deep storage of nuclear waste. During 1981-1993, this program evaluated the suitability of the crystalline basement as a hostrock for a repository. It included a deep drilling campaign consisting of seven boreholes and a range of geophysical tests (Thury et al., 1994). Since 2019, nine additional deep boreholeshave been drilled by Nagra in the cantons of Aargau, Schaffhausen and Zurich (Nagra, 2023). A 3D geological overview model was created from 2012-2015 for the Molasse basin as partof the EU programme ”INTERREG IV B Alpine Space”. The project is called ”GeoMol” and was launched to help with the assessment of geopotential for sustainable planning andmanagement of natural re- sources in the Alpine foreland basins. In addition, a detailed 3D geological model (GeoMol 17) of the Swiss Plateau was developed in a separate project. Theresults of the project are the first steps towards systematically describing and visualising Switzerland’s subsurface. Various

geological and tectonic maps, geological profiles, drillingdata, seismic sections and interpretations and other surface maps served as the data basis for this 3D model. A numerical calculation of uncertainty is not possible because 95 % of allthe used data was provided by third parties. The potential of errors within this model must certainly be considered when using this data for economical purposes (Allenbach, 2017). Forthe southern part, only individual deep wells with temperature and depth information are available, especially for some of the valleys (Swisstopo, 2023b). This lack of informationmakes the extrapolation of temperature at depth more complicated.

The first step before inter- and extrapolating the temperature was to plot all temperatures at given depths in a diagram shown below. The geothermal gradient was then determined forthree different depths using three distinct linear regression lines- one between 0 °C and 60 °C, one between 60 °C and 100 °C and one line between 100 °C and 150 °C. The plot hasmuch more values for exactly 60 °C, 100 °C and 150 °C because Swisstopo provides isotherm layers for the depth of the respective temperatures in the Molasse basin. The regressionlines show that the thermal gradient decreases by depth (Swisstopo, 2022a). The depths to a certain temperature are provided in metres above sea level (m a.s.l.). Based on that,artificial temperature points were added for areas where the data density was small. The depth for the 60 °C, 100 °C and 150 °C isotherms were calculated with the obtained gradients(see above). The aim was to fill data gaps and obtain a more meaningful extrapolation in GIS, especially in areas of high topography differences. All calculated temperatures wereloaded into the ArcGIS programme 11 with the corresponding coordinates.

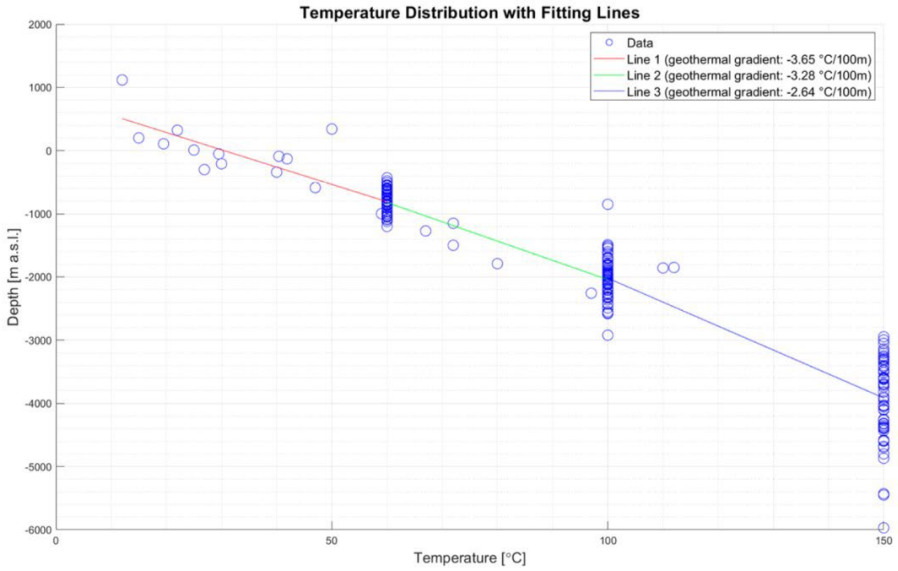

Figure 29: Geothermal gradient derive from all depth-temperature values in Merkofer, (2023)